



**Tidally-induced variations of pH at the head of the
Laurentian Channel.**

Journal:	<i>Canadian Journal of Fisheries and Aquatic Sciences</i>
Manuscript ID	cjfas-2017-0007.R2
Manuscript Type:	Article
Date Submitted by the Author:	31-Jul-2017
Complete List of Authors:	Mucci, Alfonso; McGill University, Earth and Planetary Sciences Levasseur, Maurice; Universite Laval Gratton, Yves; Institut national de la Recherche Scientifique Martias, Chloé; McGill University, Earth and Planetary Sciences Scarratt, Michael; Fisheries and Oceans Canada Gilbert, Denis; Fisheries and Oceans Canada Tremblay, Jean-Éric; Universite Laval Ferreyra, Gustavo; 5- Québec-Océans et Institut des Sciences de la Mer de Rimouski Lansard, Bruno; CNRS, 6- Laboratoire des Sciences du Climat et de l'Environnement
Is the invited manuscript for consideration in a Special Issue? :	N/A
Keyword:	Laurentian Channel, pH < General, Aragonite saturation state, ocean acidification, tidal mixing

SCHOLARONE™
Manuscripts

1 Tidally-induced variations of pH
2 at the head of the Laurentian Channel

3

4 Alfonso Mucci¹, Maurice Levasseur², Yves Gratton³, Chloé Martias¹, Michael Scarratt⁴,
5 Denis Gilbert⁴, Jean-Éric Tremblay², Gustavo Ferreyra⁵ and Bruno Lansard⁶

6 1- GEOTOP and Department of Earth and Planetary Sciences, McGill University, 3450
7 University Street, Montréal, QC, Canada H3A 0E8

8 2- Québec-Océan and Département de Biologie, Université Laval, 1045 Avenue de la
9 Médecine, Québec, QC, Canada G1V 2R3

10 3- Institut national de la Recherche Scientifique, Eau Terre et Environnement, 490 rue de la
11 Couronne, Québec, QC, Canada G1K 9A9

12 4- Fisheries and Ocean Canada, Maurice Lamontagne Institute, 850 Route de la Mer, Mont-
13 Joli, QC, Canada QC G5H 3Z4

14 5- Québec-Océans et Institut des Sciences de la Mer de Rimouski, 310 Allée des Ursulines,
15 Rimouski, QC, Canada G5L 3A1

16 6- Laboratoire des Sciences du Climat et de l'Environnement, avenue de la Terrasse,
17 domaine du CNRS, bât. 12, 91198, Gif-sur-Yvette, France

18

19 ABSTRACT

20 The head of the Laurentian Channel (LC) is a very dynamic region of exceptional
21 biological richness. To evaluate the impact of freshwater discharge, tidal mixing, and biological
22 activity on the pH of surface waters in this region, a suite of physical and chemical variables was
23 measured throughout the water column over two tidal cycles. The relative contributions to the
24 water column of the four source-water types that converge in this region were evaluated using an
25 optimum multi-parameter algorithm (OMP). Results of the OMP analysis were used to reconstruct
26 the water column properties assuming conservative mixing, and the difference between the model
27 properties and field measurements served to identify factors that control the pH of the surface
28 waters. These surface waters are generally undersaturated with respect to aragonite, mostly due to

29 the intrusion of waters from the Upper St. Lawrence Estuary and the Saguenay Fjord. The presence
30 of a cold intermediate layer impedes the upwelling of the deeper, hypoxic, lower pH and aragonite-
31 undersaturated waters of the Lower St. Lawrence Estuary to depths shallower than 50 meters.

32

33 RÉSUMÉ

34 La tête du chenal Laurentien est une région très dynamique d'une richesse biologique
35 exceptionnelle. Afin d'évaluer l'impact des apports en eaux douces, du mélange tidal, et de
36 l'activité biologique sur le pH des eaux de surface dans cette région, une suite de variables
37 physiques et chimiques a été mesurée dans la colonne d'eau sur deux cycles de marée. La
38 contribution relative des quatre sources d'eau-type qui convergent dans cette région a été évaluée
39 à l'aide d'un algorithme d'optimisation multi-paramétrique (OMP). Les résultats de l'OMP ont été
40 utilisés pour reconstruire les propriétés de la colonne d'eau en assumant un mélange conservateur
41 et la différence entre les propriétés issues du modèle et des mesures effectuées sur le terrain ont
42 servi à identifier les facteurs qui contrôlent le pH des eaux de surface. Les eaux de surface sont
43 généralement sous-saturées par rapport à l'aragonite, surtout à cause de l'intrusion d'eau provenant
44 de l'estuaire fluvial du Saint-Laurent et du fjord du Saguenay. La présence de la couche
45 intermédiaire froide (CIF) durant les marées de morte-eau tamponne l'acidification des eaux de
46 surface dans cette région de l'estuaire. La présence d'une couche intermédiaire froide limite la
47 remontée des eaux profondes, hypoxiques, de faible pH et sous-saturées par rapport à l'aragonite
48 de l'estuaire maritime du Saint-Laurent à des profondeurs de moins de 50 mètres.

49

50

51 INTRODUCTION

52 The oceans have absorbed approximately 30% of the anthropogenic CO₂ released to the
53 atmosphere since the beginning of the industrial revolution (Sabine et al. 2004). Consequently,
54 over the last century, the pH of the global ocean surface has decreased by an estimated 0.1 unit,
55 equivalent to a 30% increase in the proton concentration (Caldeira and Wickett 2005). The
56 increased acidity has lowered the saturation state of ocean waters with respect to calcite and
57 aragonite (the two most common CaCO₃ polymorphs that constitute the shells and skeleton of
58 many marine organisms) and, in combination with other stresses such as global warming, likely
59 affected the ecology of carbonate-secreting organisms (Fabry et al. 2008, Miller et al. 2009; Ries
60 et al. 2009; Kroeker et al. 2013) as well as non-calcifiers because pH plays a critical role in
61 mediating many physiological processes (Fabry et al. 2008; Kroeker et al. 2013).

62 The pH of surface waters in coastal systems is controlled by more dynamic processes than
63 in the open ocean. In these systems, the pH of surface waters may exhibit important short (hours)
64 and long (season) term variations in response to freshwater inputs and vertical mixing (Abril et al.
65 2000; Feely et al. 2010). Freshwater rivers and inner estuaries are typically supersaturated in CO₂
66 with respect to the atmosphere (Meybeck 1993; Raymond et al. 1997; Barth et al. 1999; Bauer et
67 al. 2013; Dinauer and Mucci 2017) as a result of inputs from their drainage basin and the activity
68 of heterotrophic organisms sustained by natural or anthropogenic terrestrial and riverine organic
69 carbon inputs (Frankignoulle et al. 1996, 1998; Feely et al. 2010). Consequently, waters are often
70 characterized by circum-neutral to slightly acidic pHs (Wallace et al. 2014) and are a net source
71 of CO₂ to the atmosphere (see compilation in Chen and Borges 2009). The high primary
72 productivity characterizing estuarine systems, in combination with their deep-water circulation,
73 favor the accumulation of respiratory CO₂ at depth in stratified estuaries and a further decrease in

74 pH (Taguchi et al. 2010; Cai et al. 2011; Mucci et al. 2011, Wallace et al. 2014; Hagens et al.
75 2015). In urbanized areas, this phenomenon can be exacerbated by eutrophication (Borges and
76 Gypens 2010; Sunda and Cai 2012; Melzner et al. 2013). Since variations in pH in coastal waters
77 are typically recurrent and of greater amplitude than those observed in the open ocean, one could
78 surmise that the estuarine biota will be more resilient to pH fluctuations than open ocean biota. In
79 order to evaluate the risk posed by ocean acidification on marine organisms in coastal systems, it
80 is thus essential to know the chemical properties of source waters, the relative contribution of each
81 to the coastal waters and their temporal variations. This knowledge is also required in order to
82 develop realistic experimental protocols to assess the sensitivity of estuarine organisms to ocean
83 acidification.

84
85 The head of the Laurentian Channel at the western limit of the Lower St. Lawrence Estuary
86 (LSLE, Figure 1) is one of the most dynamic regions of the St. Lawrence Estuary. Here, complex
87 tidal phenomena due to rapid shoaling (tidal movements, including internal tides and strong flows
88 over the steep entrance sill) generate significant mixing of near-surface waters with the deeper
89 saline waters, resulting in a nutrient-rich surface layer that sustains the feeding habitat of several
90 large marine mammals. Four different water masses converge at this location: the brackish surface
91 waters of the Upper St. Lawrence Estuary (USLE), the brackish surface waters discharged at the
92 mouth of the Saguenay Fjord, the cold intermediate layer (CIL) waters of the LSLE and the
93 hypoxic bottom waters of the LSLE (Mucci et al. 2011). With the exception of the Saguenay River
94 waters, the other water masses are supersaturated in CO₂ with respect to the atmosphere (Table 1),
95 the supersaturation having been acquired from their tributaries and/or the accumulation of
96 metabolic CO₂ from microbial respiration of autochthonous or allochthonous organic matter (Yang

97 et al. 1996; Barth et al. 1999; Wang and Veizer 2000). The objective of this study was to assess
98 how the confluence and mixing of these different water masses affect the chemical and biological
99 properties of the surface waters over two tidal cycles at a fixed station at the head of the Laurentian
100 Channel. After identifying the properties of the individual end-member water-mass types, we
101 estimated the relative contribution of each water-mass type to the surface waters at the fixed station
102 by solving for a set of linear equations for conservative and non-conservative properties. A
103 reconstruction of the water column properties at the fixed station and a comparison with field
104 measurements are used to identify factors that control the pH of surface waters in this region over
105 the study period.

106

107 **Study Site:**

108 **The St. Lawrence Estuary**

109 The St. Lawrence Estuary (SLE) receives the second largest freshwater discharge (11900 m^3
110 s^{-1}) in North America (El-Sabh and Silverberg 1990). It begins at the landward limit of the salt
111 intrusion near Ile d'Orléans and extends 400 km seaward to Pointe-des-Monts and the Gulf of St.
112 Lawrence (GSL), a semi-enclosed sea connected to the Atlantic Ocean via Cabot Strait and the
113 Strait of Belle-Isle (Fig. 1). The Upper St. Lawrence Estuary (USLE) is the relatively shallow, well
114 mixed, and fully oxygenated transition zone between the mouth of the St. Lawrence River at
115 Quebec City and the marine region ($S_p \approx 25$ and greater) beginning at Tadoussac (Fig. 1). At the
116 transition between the Upper and Lower St. Lawrence Estuary, the water column deepens from 50
117 m to 300 m over less than 20 km, in an area characterized by diverse and complex tidal phenomena
118 (Gratton et al. 1988; Saucier and Chassé 2000). The dominant bathymetric feature of the Lower
119 St. Lawrence Estuary (LSLE) is the Laurentian Channel, a 1240 km long, 250-500 m deep

120 submarine valley that extends from the edge of the eastern Canadian continental shelf, through
121 Cabot Strait, to the confluence of the St. Lawrence Estuary and the Saguenay Fjord at Tadoussac.
122 The water column in the LSLE is strongly stratified and, throughout most of the year, is
123 characterized by three distinct layers (Dickie and Trites 1983): (1) a thin surface layer (25-50 m
124 deep) of low salinity (27-32) flowing seaward, (2) an intermediate cold (-1 to 2°C) and saline
125 (31.5-33) layer (CIL) that originates in the Gulf in the winter, extends to about 150 m depth, and
126 flows landward, and (3) a warmer (4-6°C) and saltier (34-34.6) deep layer (150+ m) that flows
127 landward (El-Sabh and Silverberg 1990). Two typical vertical profiles taken at one of our sampling
128 stations, station 1B (Figure 1b: 48°19.8'N, 069°17.4'W; June 11, 2013; 16:48GMT) and at station
129 18 (Figure 1a: 49° 16.0, 064° 16.5; June 7, 2013; 16:01 GMT) are reproduced in Figure 2. The
130 surface layer displays large seasonal variations in temperature and salinity due to atmospheric and
131 buoyancy (i.e., runoff events) forcing. In winter, the surface layer becomes progressively colder
132 and denser, as tributary flow decreases, air temperatures plummet, and ice forms, until it merges
133 with the intermediate layer (Gilbert and Pettigrew 1997; Galbraith 2006). The deep waters are a
134 mixture of Labrador Current and North Atlantic Central waters whose proportions vary on a
135 decadal or secular timescale (Bugden 1991; Gilbert et al. 2005). The transit time of a parcel of
136 water between the seaward end of the Laurentian Channel at the edge of the continental shelf and
137 the head of the Channel at Tadoussac has been estimated at 4 to 7 years (Bugden 1991, Gilbert
138 2004) whereas the mean age of the deep waters of the LSLE is believed to be ~20 years (Mucci et
139 al. 2011). Given the properties of the source waters, benthic and pelagic respiration along the
140 Channel, and their mean age, the bottom waters of the LSLE are hypoxic (<20% oxygen saturation;
141 Gilbert et al. 2005), charged with metabolic CO₂ and therefore acidified (Mucci et al. 2011). The
142 landward end of the Laurentian Channel marks the transition from the Lower to the Upper St.

143 Lawrence Estuary, the mouth of the Saguenay Fjord, and the marine region ($S_P \approx 25$ and greater)
144 beginning at Tadoussac (Fig. 1). Typical semi-diurnal (M2) tidal current amplitudes in the LSLE
145 are on the order of 0.2 m s^{-1} (Saucier and Chassé 2000), so that tidal excursions are on the order
146 of 3 km.

147 *The Saguenay Fjord*

148 The Saguenay Fjord is a 93 km long, 1-6 km wide and 275 m deep U-shaped submerged
149 valley, bounded by sheer, vertical walls that reach up more than 300 m above the water line.
150 Situated approximately 150 km northeast of Quebec City on the north shore of the St. Lawrence
151 Estuary, it connects with the estuary at Tadoussac through a 20-m deep sill. Its bathymetry is
152 defined by three basins separated by two sills at 60 and 120 m depth, located approximately 20 km
153 and 30 km, respectively, from the mouth of the fjord. A short account of its geological history and
154 physiographic features can be found in Schafer et al. (1990) and Locat and Levesque (2009).

155 The water column of the Saguenay Fjord is characterized by a sharp pycnocline that
156 separates two distinct water masses. The thick bottom layer is well-mixed and oxygenated, with
157 waters penetrating landward from the St. Lawrence Estuary as they episodically spill over the sills
158 (Therriault and Lacroix 1977; Siebert et al. 1979; Stacey and Gratton 2001; Bélanger 2003; Belzile
159 et al. 2015). Bottom-water salinities are approximately 30.5 (Mucci et al. 2000), with temperatures
160 ranging from 0.4 to 1.7°C (Fortin and Pelletier 1995). The surface layer consists of brackish waters
161 ($S_P \sim 0-10$) resulting from the turbulent mixing of the outflow from the Saguenay River (and smaller
162 tributaries such as the Valin, Ha! Ha! and Mars Rivers) and the underlying marine waters. The
163 thickness of the surface layer, perhaps best defined by the depth of the 18.00 sigma-tee isopycnal,
164 typically increases towards the mouth of the fjord, but pinches off towards the surface at high tide

165 or when denser waters overflow the entrance sill. The surface water temperatures range from
166 freezing in winter to 16°C in summer (Fortin and Pelletier 1995). Detailed hydrographic
167 characteristics of the fjord can be found in Schafer et al. (1990) and Gratton et al. (1994).

168 Figure 3 shows a 3-day average of sea-surface temperatures derived from satellite data
169 (OGSL 2014). A prominent tongue of cold surface waters due to upwelling and tidal mixing
170 extends from the head of the Laurentian Channel (near Tadoussac) to about Rimouski. Our fixed
171 station is located at the northern edge of this cold tongue.

172 **Methods**

173 *Water column sampling*

174 On June 10-15, 2013, we sampled the whole water column at six stations and surface waters
175 (3 – 5 m below the surface) at four stations along a saw-tooth transect at the head of the Lower St.
176 Lawrence Estuary (LSLE), the mouth of the Upper St. Lawrence Estuary (USLE) and the mouth
177 of the Saguenay Fjord (Figure 1). In addition, we sampled the whole water column every four
178 hours and surface waters (~3 m) every two hours over 50 hours at a fixed station (48°11.2'N,
179 69°34.4'W) a few kilometers east of the fjord's mouth in the northern half of the head of the LSL
180 in order to characterize changes in the properties of these surface waters over two tidal cycles.
181 Finally, the whole water column at four stations (Stations 23, 22, 20, 18) in the LSL and western
182 Gulf of St. Lawrence was sampled on an earlier cruise (June 3-8, 2013) and these results served to
183 better define the properties of the source-water types encountered at the fixed station (see *Water*
184 *mass analysis* section below). Water samples were collected using a 12-Niskin bottle/CTD
185 (SeaBird SBE 911) rosette sampler onboard the R/V Coriolis II. Sampling depths were typically,
186 3, 10, 20, 40, 60, 80, 100, 150 m deep, in addition to 15 m above the bottom. The pH (on the NBS

187 scale - pH_{NBS}), dissolved oxygen (DO), temperature and conductivity probes were calibrated by
188 the manufacturer during the winter months preceding the cruise. Nevertheless, discrete samples
189 were taken from the Niskin bottles for laboratory measurements of pH (total proton concentration
190 scale – pH_{T}), DO and salinity and the CTD records re-calibrated post-cruise. Additional surface
191 water samples were collected, on distinct outings, in Chicoutimi (Saguenay River end-member)
192 and near Quebec City (St. Lawrence River end-member) during or within a week of the research
193 cruise.

194

195 *Analytical methods*

196 Discrete salinity samples taken throughout the water column were analyzed on a Guildline
197 Autosal 8400 salinometer calibrated with IAPSO standard seawater. The instrument has a
198 theoretical accuracy $< \pm 0.002$. Dissolved oxygen (DO) concentrations were determined by
199 Winkler titration (Grasshoff et al. 1999) of water samples recovered from the Niskin bottles. The
200 relative standard deviation, based on replicate analyses of samples recovered from the same Niskin
201 bottle, was better than 1%. These measurements further served to calibrate the SBE-43 oxygen
202 probe mounted on the rosette.

203 Water samples destined for pH and titration alkalinity (TA) measurements were transferred
204 directly from the Niskin bottles to, respectively, 125 mL plastic bottles without headspace and 250
205 mL glass bottles, as soon as the rosette was secured onboard. In the latter case, a few crystals of
206 HgCl_2 were added before the bottle was sealed with a ground-glass stopper and Apiezon[®] Type-
207 M high-vacuum grease.

208 The pH of the 125 mL samples was determined onboard using a Hewlett-Packard UV-
209 Visible diode array spectrophotometer (HP-8453A) and a 5-cm quartz cell after thermal
210 equilibration of the sampling bottles in a constant temperature bath at $25.0 \pm 0.1^\circ\text{C}$. Phenol red
211 (PR; Robert-Baldo et al. 1985) and *m*-cresol purple (mCP; Clayton and Byrne 1993) were used as
212 indicators. The absorbance at the wavelengths of maximum absorbance of the protonated (HL)
213 and deprotonated (L) indicators were measured and recorded. A similar procedure was carried out
214 several times each day using TRIS buffers prepared at practical salinities (S_P) of ~ 35 and ~ 25
215 (Millero 1986). The pH on the total proton concentration scale (pH_T) of the samples and buffer
216 solutions were calculated according the equation of Byrne (1987). The salinity-dependence of the
217 dissociation constants and molar absorptivities of the indicators were taken from Robert-Baldo et
218 al. (1985) for phenol red and from Clayton and Byrne (1993) for *m*-cresol purple. The salinity-
219 dependence of the phenol red indicator dissociation constant and molar absorptivities was
220 extended (from $S_P = 5$ to 35; Bellis 2002) to encompass the range of salinities encountered in this
221 study, but computed pH_T s from the revised fit were not significantly different from those obtained
222 with the relationship provided by Robert-Baldo et al. (1985). All measurements were converted to
223 the total proton scale using the salinity of each sample and the HSO_4^- association constants given
224 by Dickson (1990). Reproducibility and accuracy of our TRIS buffer measurements were on the
225 order of 0.005 pH units or better. The computed pH_T s at 25°C and 1 atmosphere total pressure
226 were then used in combination with the measured TA to calculate the pH_T s at the in-situ
227 temperature and pressure using the Microsoft Excel version of CO2SYS (Pierrot et al. 2006), based
228 on the original algorithm of Lewis and Wallace (1998), and the carbonic acid dissociation
229 constants of Cai and Wang (1998), the total boron concentration $[\text{B}]_T$ value from Uppström (1974),
230 and the standard acidity constant of the HSO_4^- ion ($K(\text{HSO}_4)$) from Dickson (1990).

231 The titration alkalinity (TA) was determined at the land-based laboratory within one week
232 of sampling by open-cell automated potentiometric titration (Titrilab 865, Radiometer®) with a pH
233 combination electrode (pHC2001, Red Rod®) and a dilute (~0.025N) HCl titrant. The latter was
234 calibrated against Certified Reference Materials (CRM Batch#94, provided by A. G. Dickson,
235 Scripps Institute of Oceanography, La Jolla, USA). Samples were drawn from the 250 mL sample
236 bottle and weighed on an analytical balance to ± 0.1 mg. The average relative error, based on the
237 average relative standard deviation on replicate standard and sample analyses, was better than
238 0.15%.

239

240 *Nutrients*

241 Subsamples for nutrient determinations were filtered through a 0.45 μm disposable syringe
242 filter to remove particles. Dissolved NH_4^+ concentrations were determined immediately onboard
243 with the fluorometric method described by Holmes et al. (1999), with a detection limit of 0.01 μM .
244 For nitrate, nitrite, soluble reactive phosphorus (SRP) and soluble reactive silicon (SRS), filtered
245 samples were collected into acid-washed 15-ml polyethylene tubes and quickly frozen and stored
246 at -20°C . Back at home laboratory, frozen samples were rapidly thawed and concentrations of
247 inorganic nutrients were determined using the routine colorimetric method adapted from Hansen
248 and Koroleff (2007) with a Bran and Luebbe Autoanalyzer III. The analytical detection limit was
249 0.02 μM for nitrite, 0.04 μM for nitrate+nitrite (hereafter dissolved inorganic nitrogen, DIN), 0.05
250 μM for SRP and 0.1 μM for silicate.

251

252 *Isotopic composition*

253 Water samples for isotopic analysis were collected in 13 mL screw-top plastic test tubes.
254 The stable oxygen isotopic composition ($\delta^{18}\text{O}$) of the water samples was analyzed at the GEOTOP-
255 UQAM stable isotope laboratory. 200- μL aliquots of the water samples and two laboratory internal
256 reference waters were transferred into 3-mL vials stoppered with a septum cap. The vials were
257 then placed in a heated rack maintained at 40°C. Commercially available CO_2 gas was introduced
258 in all the vials using a Micromass AquaPrep and allowed to equilibrate for 7 hours. The headspace
259 CO_2 was then sampled by the Micromass AquaPrep, dried on a -80°C water trap, and analyzed on
260 a Micromass Isoprime universal triple collector isotope ratio mass spectrometer in dual inlet mode.
261 Data were normalized against the two internal reference waters, both calibrated against V-SMOW
262 and V-SLAP. Data are expressed in ‰ with respect to V-SMOW, and the average relative standard
263 deviation on replicate measurements of sample waters is better than 0.05‰.

264

265 *Water mass analysis*

266 The water mass analysis was performed using the optimum multi-parameter algorithm
267 (OMP) of Karsteen and Tomczak (1999), originally developed by Tomczak (1981). OMP analysis
268 is based on a simple model of linear mixing. It assumes that all water mass properties undergo the
269 same mixing process, i.e. their mixing coefficients are identical, as is the case in turbulent mixing.
270 The spatial water mass distribution can therefore be determined through a linear set of mixing
271 equations. OMP determines the contributions of pre-defined end-member water masses (so called
272 source-water types or SWT) to a sample. The SWT contributions or fractions (X_i) for each data
273 point are obtained by finding the best linear mixing combination in parameter space defined by
274 temperature, salinity, oxygen, total alkalinity and $\delta^{18}\text{O}$ which minimizes the residuals in a non-

275 negative least squares analysis. The solution includes two physically realistic constraints: (i) the
276 contributions from all sources must add up to 100%, and (ii) all contributions have to be non-
277 negative.

278 Based on the description of the water circulation in the LSLE, four different source-water
279 types contribute to the water column properties at the head of the Laurentian Channel: the
280 freshwaters of the St. Lawrence and Saguenay Rivers, the saline and cold intermediate layer water
281 and the upwelling saline hypoxic bottom water of the LSLE. Even though the properties of the
282 source-water types are variable in both space and time, we use the dataset acquired during this
283 study as well as data acquired a week before on another cruise along a seaward transect through
284 the Lower Estuary and Gulf of St. Lawrence to define the most representative properties for each
285 source-water type (Table 1). This allows the direct comparison of the water mass fractions and
286 their vertical distribution at the time of sampling. Whereas OMP analysis was initially used to
287 distinguish and calculate the relative contributions of each source-water type in a parcel of water
288 using temperature, practical salinity (S_P) and nutrient data (Mackas et al. 1987), in this study, we
289 used S_P , the titration alkalinity (TA), and $\delta^{18}\text{O}(\text{H}_2\text{O})$ as conservative tracers as well as temperature
290 and dissolved O_2 (DO) concentrations as non-conservative tracers, to constrain the water mass
291 analysis. Non-conservative tracers should be applied with caution in OMP, because of temporal
292 and spatial variability, particularly in the surface waters. For example, the temperature of the
293 Saguenay River water ranges from 0°C in winter to $+16^\circ\text{C}$ in summer whereas the temperature of
294 the St. Lawrence River ranges from 0°C in winter to $>20^\circ\text{C}$ in summer. Dissolved O_2 concentration
295 was also used as a non-conservative tracer, because it is a function of temperature (e.g. O_2
296 solubility increases with decreasing temperature and salinity) and, like ΣSi and SRP, also a
297 function of primary production and biological respiration. Consequently, end-member matrix and

298 sample observations were multiplied by a diagonal weight matrix to account for differences in
299 tracer reliability, environmental variability, and precision of the data (Table 2). The error
300 associated with the water mass fraction analysis was estimated to be about $\pm 10\%$ of the fractional
301 values (Macdonald et al. 1989; Lansard et al. 2012).

302

303 **Results and discussion**

304 *Variations of the water properties over two tidal cycles*

305

306 Figures 4a-l show time-series of water property profiles from the CTD (1-m resolution) at
307 the fixed station (SF) over two tidal cycles from June 13 to June 15, 2013. Results of the OMP
308 analysis are presented in Figures 5a-d.

309 The tides are very strong in the fixed station region. The impact of tides on the local
310 circulation is described in detail in Saucier and Chassé (2000). Near the SF, the tidal elevation in
311 the channel can be larger than 5 m (unpublished data) at the spring tide. Mertz and Gratton (1990)
312 reported internal oscillations on the order of 40-60 m over a tidal semi-diurnal cycle. Similar
313 oscillations can be observed on Figures 4a,b,c. The cold, upwelled water can reach the surface and
314 be observed flowing downstream as on Figure 3. As observed on this figure, our SF is located at
315 the edge of these cold surface waters.

316 Surface salinities decrease and temperatures increase during ebb tide (Figs. 4a,b), as
317 freshwaters from the Saguenay and the St. Lawrence Rivers, but mostly of the latter (Figs. 5a,b),
318 intrude into the Lower St. Lawrence Estuary (LSLE) and at our fixed station. The intrusion is
319 detectable to depths of about 30 m and accompanied by a slight (less than 0.1 pH unit) decrease in
320 pH (Fig. 4f). Higher salinity, lower temperature and higher pH waters impinge closer to the surface

321 during the flood tide whereas patches of low pH waters from the Saguenay Fjord persist at the
322 surface well into flood tide (Figs. 4a,b,f). The former correspond to the upwelling/invasion of the
323 cold intermediate layer (CIL) nearly up to the surface where it accounts for more than 80% of the
324 mixture (Fig. 5c). Temporal variations of the surface-water titration alkalinity (TA) and dissolved
325 inorganic carbon (DIC) concentrations are almost perfectly correlated with those of the salinity
326 (Figs. 4e,g). Temporal variations of the surface-water major nutrient concentrations are more
327 diffuse, but are nonetheless either correlated (SRP ($r^2 = 0.63$); Fig. S1) or anti-correlated (DIN (r^2
328 $= 0.46$) and ΣSi ($r^2 = 0.62$); Fig. S1) to salinity in the top 3 m, reflecting the differential input from
329 the freshwaters (Saguenay and St. Lawrence Rivers) and the CIL.

330 Irrespective of the tide, dissolved oxygen concentrations remain high ($> 260 \mu\text{M}$, Fig. 4d)
331 throughout the top 80-100 m of the water column. Likewise, the computed pCO_2 in the top 80 m
332 of the water column is slightly supersaturated with respect to the atmosphere ($\sim 400 \mu\text{atm}$) and
333 shows few discernible features, except for a greater pCO_2 supersaturation at low tide when the
334 contribution of freshwaters from the St. Lawrence River and Saguenay Fjord, both of which are
335 rich in metabolic CO_2 and dissolved silicate (as well as ammonium in the latter case) relative to
336 the CIL, are maximum (Fig. 5a,b).

337 As expected, below 150 m depth, hypoxic bottom waters are dominated by Atlantic waters
338 that enter the Gulf and Estuary through Cabot Strait. These waters intrude to depths as shallow as
339 80 m at high tide (Fig. 5d).

340

341 *pH in the surface waters*

342

343 The pH_T of the surface waters (top 3 m) varied from 7.855 to 7.934 during the 50-hour
344 survey, nearly as much as the world's oceans have experienced as a result anthropogenic CO_2
345 uptake over the last century (Caldeira and Wickett 2005). The pH_T of surface waters is determined
346 by the relative contribution of the three source-water types (SLW, SRW, and CIL), itself
347 determined in great part by tidal mixing, as well as by gas exchange with the atmosphere, the
348 addition of metabolic CO_2 through bacterial respiration and biological uptake of CO_2 through
349 photosynthesis. Mucci et al. (2011) reported on the variation of surface-water (0-16 m depth
350 interval) pH over the period 1933-2009 (also limited to the ice-free season) in the Lower St.
351 Lawrence Estuary (LSLE). Unlike the deeper waters that have become hypoxic and acidified, the
352 pH of surface waters shows no systematic variations over this period. Although the intra-annual
353 variability reaches ~ 0.1 pH unit, the inter-annual variability is nearly null (slope = 0, $p > 0.05$; i.e.,
354 no statistically significant temporal variation). Along the Estuary and Laurentian Channel, pH
355 variations can exceed the intra-annual variability in the LSLE as the salinity and balance between
356 respiration and photosynthetic rates vary (Dinauer and Mucci 2017).

357

358 Throughout the three-day survey, waters in the surface layer (0-3 m) at the sampling sites
359 were always supersaturated in CO_2 (443-550 μatm) with respect to the atmosphere at the time of
360 sampling. The saturation state of the surface mixed layer water with respect to aragonite, given by:

$$361 \quad \Omega_A = [\text{Ca}^{2+}][\text{CO}_3^{2-}]/K_A^* \quad (1)$$

362 where K_A^* is the stoichiometric solubility of aragonite at the in-situ temperature and salinity and
363 1 atmosphere total pressure (Mucci, 1983), varied little during the sampling period and was close
364 to saturation ($\Omega_A = 0.88$ to 1.02 , 0.95 ± 0.03 , $n=27$, Fig. 6), but fell slightly below saturation (as
365 low as $\Omega_A = 0.88$) at low tide. Given the ratio of the stoichiometric solubility constants (K_A^*/K_C^*

366 = 1.5; Mucci, 1983), the saturation state of the surface waters with respect to calcite was close to
367 1.5. Deeper waters became undersaturated with respect to aragonite below 60-80 m reaching
368 saturations as low as 0.70, but remained supersaturated with respect to calcite to the bottom at the
369 fixed station.

370

371 *Validation of the OMP analysis*

372

373 Using the results of the OMP analysis and the source-water type properties in Table 1, the
374 total alkalinity (TA), DIC and nutrient concentrations of each discrete water sample at the fixed
375 station was calculated, over the whole time series, assuming conservative mixing (i.e., closed
376 system). These computed values were then used as input parameters into CO2SYS to calculate the
377 pH_T of the mixture and results compared to measured values. Differences between the calculated
378 and observed surface waters properties are compiled in Table 3; these reflect changes to the water
379 properties beyond those that can be accounted for by mixing of the source waters. The ΔpH_{calc} -
380 meas values (thereafter referred to as ΔpH_T) of the surface waters (1-3 m) are all negative (-0.004
381 to -0.066), indicating that either CO_2 was lost by ventilation to the atmosphere or taken up by
382 photosynthesis during our observation period. As indicated above, surface waters remained
383 supersaturated with respect to the atmosphere throughout the sampling period and thus served as
384 a net source to the atmosphere. CO_2 exchange across the air-sea interface is, however, a slow
385 process, much slower than for oxygen and most other gases (Zeebe and Wolf-Gladrow, 2001),
386 particularly under the low wind conditions (~5-28 knots) experienced during the cruise. Given
387 these wind speeds, the parameterizations of Raymond and Cole (2001) and Wanninkhof (2014)
388 for the gas transfer velocity, an average surface water pCO_2 of 499 ($\pm 26 \mu atm$) during the sampling

389 period, and a local atmospheric $p\text{CO}_2$ of 391 μatm , we estimated the air-sea CO_2 efflux (loss of
390 CO_2 to the atmosphere) to range between 2.6 and 4.8 $\text{mmol m}^{-2} \text{d}^{-1}$. Over our sampling period, the
391 loss of CO_2 to the atmosphere did not affect the DIC budget significantly (less than 1 $\mu\text{mol/kg}$)
392 and would have increased the surface-water pH by at most 0.003 unit, slightly below the
393 uncertainty of our field measurements. The positive $\Delta p\text{CO}_2$, ΔDIN and ΔSRP values (net DIC and
394 nutrient uptake) as well as negative ΔDO values (net oxygen production) in the surface waters are
395 clear evidence that photosynthesis (CO_2 uptake, pH increase) dominated over respiration (CO_2
396 production and pH decrease) and ventilation over the whole sampling period (Table 3).
397 Unfortunately, in the absence of independent estimates of the absolute photosynthetic and/or
398 respiration rates, we can only determine which of these two processes dominates. It is also
399 interesting to note that, despite the large uncertainties in the model and the intrinsic patchiness of
400 our measurements, the average $\Delta\text{DIN}:\Delta\text{SRP}$ ratio (11 ± 4) nearly corresponds to the Redfield
401 stoichiometry of 15-16 (Redfield et al. 1963) and the DIN: SRP ratio (12, $r^2 = 0.79$) below 30 m
402 depth in the LSLE. When the surface-water ΔpH_T , ΔDIN , ΔSRP , $\Delta\Sigma\text{Si}$ and ΔDO values are plotted
403 as function of the time of the day, no systematic variation with daylight is apparent (Fig. 7). The
404 study region is known to be an area of high primary productivity, notably during the spring tide
405 periods when upwelling and internal waves amplitude are maximum (Therriault and Levasseur
406 1985, Levasseur and Therriault 1987), but can be strongly suppressed spring fresh-water runoff
407 (Zakardjian et al. 2000). Hence, it is not surprising that we observe net autotrophy in the surface
408 waters but our conservative mixing model is not able to resolve the diurnal cycle of photosynthesis
409 and respiration, likely because it is not sensitive enough. Note that we have not modeled temporal
410 variations of pH below the surface mixed layer (SML) because, as shown in Figure 5, below $\sim 30\text{m}$,
411 the water column is entirely dominated by two water masses, the CIL between 30 and 50 m and

412 Atlantic (deep LSLE) waters below 150 m. In other words, with the exception of the SML,
413 significant variations in water column composition in response to the tide are only found between
414 50 and 150 m. Given that these waters are isolated from the atmosphere (no gas exchange), below
415 the euphotic zone (no photosynthesis), and respiration rates are negligible on the time scale of the
416 experiments, temporal variations are simply due to tidal oscillations.

417
418 *Susceptibility of estuarine waters to acidification resulting from direct anthropogenic CO₂ uptake*

419
420 As noted above, most inner (river-dominated) estuaries are net sources of CO₂ to the
421 atmosphere (Cai and Wang 1998; Chen and Borges 2009; Regnier et al. 2013). Their elevated DIC
422 enrichments and pCO₂ supersaturations can mainly be attributed to the *in situ* microbial
423 degradation of internally and externally supplied organic carbon and the lateral transport of
424 inorganic carbon from rivers, coastal wetlands and ground waters (Bauer et al., 2013). Thus, these
425 waters do not directly take up anthropogenic CO₂ from the atmosphere. Nonetheless, there have
426 been several reports of weak CO₂ uptake by strongly stratified and/or marine-dominated (outer)
427 estuaries (Koné et al. 2009; Maher and Eyre 2012; Cotovicz Jr. et al. 2015), including the Lower
428 St. Lawrence Estuary (Dinauer and Mucci 2017). The resistance of these estuarine waters to a
429 decrease in pH in response to CO₂ uptake is equated to a multiple of the carbonate ion
430 concentration ([CO₃²⁻]) (Stumm and Morgan 1996), and the latter, within the pH range of most of
431 these (7.5 < pH_T < 8.1), is approximated by TA – DIC (Broecker and Peng 1982).

432 Variations of the saturation state of waters with respect to aragonite (or calcite) depend
433 on the calcium and carbonate ion concentration product and the mineral solubility under in-situ
434 conditions (Eqn. 1). The [Ca²⁺] in estuarine waters is determined by the composition and mixing

435 ratio of the freshwater and seawater end-members, but given its high and conservative
436 concentration in seawater, the freshwater signature typically becomes indistinguishable (within a
437 1% deviation of the diluted seawater value) from that of seawater above a salinity of ~14. The
438 minimum salinity measured during our survey was 24.82. Hence, the $[Ca^{2+}]$ can accurately be
439 estimated from the measured salinities, i.e., $[Ca^{2+}] = S_P * 0.01028/35$ (Millero 2013). Both $[Ca^{2+}]$
440 and K_A^* increase with salinity and to a similar extent (31% and 32.5%, respectively, over the range
441 of salinities encountered during our study), so that Ω_A varies almost exactly with the $[CO_3^{2-}]$.
442 Hence, again, the impact of CO_2 uptake on the saturation state of most marine-dominated estuaries
443 is almost exclusively related to changes in $[CO_3^{2-}]$ which, as noted above, can be approximated by
444 $(TA - DIC)$.

445

446 *Biological response of some local $CaCO_3$ -secreting invertebrates to ocean acidification*

447

448 Atmospheric CO_2 uptake lowers the pH, the carbonate ion concentration and saturation
449 state of natural waters with respect to calcite and aragonite (Ω_C and Ω_A , respectively).
450 Consequently, the ability of many organisms to calcify is reduced by a decrease in the saturation
451 state of the waters and sediments they inhabit (Gazeau et al. 2013; Clements and Hunt 2017).
452 Aragonite being 50% more soluble than calcite (Mucci, 1981), organisms whose shells or skeletons
453 are partially or wholly aragonitic will be more susceptible to acidification.

454 Aragonite-undersaturated waters ($\Omega_A < 1$) dominate the top 20 metres of the water
455 column at the head of the Laurentian Channel except when the CIL intrudes almost up to the
456 surface at high tide. Below the CIL, the aragonite saturation depth ($\Omega_A = 1$) oscillates between 40
457 and 90 m reaching the shallowest depths at high tide when these waters are brought closer to the

458 surface. Hence, the recruitment, growth, metabolism and survival of calcifying invertebrates and
459 other benthic organisms exposed to these waters could be deleteriously affected (Parker et al. 2012;
460 Gazeau et al. 2010; Talmage et al. 2010; Kuhihara 2008).

461 Commercial harvesting of bivalve shellfish (scallops, soft-shell clams, mussels, Atlantic
462 surf-clams, Atlantic razor clams), echinoids (green sea urchin), and gastropods (common whelk)
463 in Quebec sustains several coastal communities with annual landings in the range of 2.5-4 million
464 dollars (DFO; [http://www.qc.dfo-mpo.gc.ca/peches-fisheries/recreative-recreational/mollusque-](http://www.qc.dfo-mpo.gc.ca/peches-fisheries/recreative-recreational/mollusque-mollusc-eng.asp?p=/peches-fisheries/recreative-recreational/mollusque-mollusc-eng.html)
465 [mollusc-eng.html](http://www.qc.dfo-mpo.gc.ca/peches-fisheries/recreative-recreational/mollusque-mollusc-eng.html)).

466 Scallops (e.g., *Chlamys islandica*), soft-shell clams (e.g., *Mya arenaria*), the common whelk (e.g.,
467 *Buccinum undatum*) and the green sea urchin (e.g., *Strongylocentrotus droebachiensis*) are found
468 on the seafloor near the head of the Laurentian Channel and, with the exception of scallops (Hutin
469 et al. 2005), are mostly harvested from no more than 20 m depth (Bernard Saint-Marie, DFO, pers.
470 comm.). Except for the green sea urchin, harvesting of the other species has declined steadily
471 since the beginning of the new millennium and there are currently no active commercial shellfish
472 fisheries in this region while recreational harvesting of scallops is now forbidden. The shells of
473 most bivalves and whelks found in the study area are composed of a combination of calcite and
474 aragonite (micro-) structural components (groups and layers) whereas the body and spines of sea
475 urchins are typically composed of high-magnesium calcite (more soluble than aragonite) and, thus,
476 their constant exposure to the aragonite-undersaturated (corrosive) waters in the top 20 m of the
477 water column and along the shorelines in the vicinity of the study area could possibly have
478 contributed, along with overfishing (Archambault and Goudreau 2006), to their decline. Since the
479 habitat of scallops extends to depths of 80 meters (the largest scallop bed in the vicinity of
480 Tadoussac is situated 5-10 km downstream of Ile Rouge in 40-80 m of water; Hutin et al. 2005),

481 this would put them well into the aragonite-undersaturated (corrosive) waters found below the
482 CIL.

483 To our knowledge, no specific study of the impacts of elevated pCO₂s (lower pH and
484 Ω_A) has been carried out on *Chlamys islandica* and *Buccinum undatum*, but studies conducted on
485 other species of scallops and whelk have reported deleterious effects on calcification and growth
486 of the former and the nutritional properties of the latter (Tate et al. 2017; Andersen et al. 2013).
487 Conversely, in addition to lowered calcification rates, the impacts of elevated pCO₂ on *Mya*
488 *arenaria* were found to extend to their burrowing behavior, post-settlement dispersal (Clements et
489 al. 2016) as well as predator-prey interactions (Glaspie et al. 2017) whereas, in the case of
490 *Stromylocentrotus droebachiensis*, the effects extend to the fecundity, gonad growth, feeding rates
491 and susceptibility to metal toxicity (Lewis et al. 2016; Dupont et al. 2013; Siikavuopio et al. 2007).

492 Notwithstanding the potential impact of ocean acidification (OA) on the organisms
493 listed above, one should consider that these organisms may have, over time, developed a tolerance
494 or acclimatized to the high-amplitude and high-frequency (diurnal, seasonal) variations of
495 environmental variables (T, S, pH) encountered in dynamic estuaries such as the USLE, as has
496 been demonstrated in long-term exposures to elevated pCO₂ (Dupont et al. 2013; Moulin et al.
497 2015; Uthicke et al. 2016). Whereas the above discussion is limited to commercially-harvested
498 CaCO₃-secreting benthic organisms, OA may impact on the metabolic activity (e.g., survival,
499 growth, reproduction) of many other organisms, but an expanded discussion of these would be
500 well beyond the scope of this paper given the range of responses documented in the literature (e.g.,
501 Doney et al. 2009).

502

503 In summary, the pH of surface waters at the head of the Laurentian Channel is modulated
504 by tides and mixing of three source–water types, the relatively high alkalinity (TA) and dissolved
505 inorganic carbon (DIC)-rich water of the St. Lawrence River (TA-DIC <0), the TA and DIC-poor
506 water of the Saguenay River (TA-DIC) <0) and saline waters of the TA and DIC-rich cold
507 intermediate layer (CIL) of the St. Lawrence Estuary (TA-DIC) >0) that upwell in this region.
508 Consequently, in-situ pH_T values lower than 8.0 are found below the CIL or 80 m depth and in the
509 top 30 m of the water column. Nevertheless, upwelling of the TA-rich CIL and mixing with lower
510 salinity waters near the surface limit pH excursions within a narrow range (7.86 to 7.93) as the
511 (TA-DIC) of the mixture at our study site (head of the Laurentian Channel) was always positive.
512 The presence of the CIL also appears to impede the upwelling of the hypoxic, CO₂-rich and
513 aragonite-undersaturated bottom waters of the Lower St. Lawrence Estuary (LSLE) to depths
514 shallower than about 80 m (Figure 5), although the large density gradient, as well as the tidal (~5
515 m) and internal-wave amplitudes (maximum 50-60 m), would not allow bottom waters to intrude
516 at the surface. The CIL is not unique to the SLE as similar layers are common in other subpolar
517 basins (Osafune and Yasuda 2006; Cyr et al. 2015). Organisms living within the first 20 meters of
518 the water column at the head of the Laurentian Channel are bathed, at low tide, by aragonite-
519 undersaturated waters ($\Omega_A < 1$) intruding from the St. Lawrence and Saguenay Rivers. Likewise,
520 those that live below 80 meters depth, below the CIL, such as the largest scallop bed in the area,
521 are continuously exposed to the aragonite-undersaturated bottom waters ($\Omega_A < 1$) of the LSLE that
522 upwell up to nearly 40 metres from the surface at high tide. Whereas the growth, recruitment, and
523 other metabolic functions of CaCO₃-secreting invertebrates exposed to these aragonite-
524 undersaturated waters may be deleteriously affected, some of these organisms may have, over
525 time, developed a tolerance or acclimatized to the high-amplitude and high-frequency (diurnal,

526 seasonal) variations of environmental variables (T, S, pH) encountered in this dynamic
527 environment.

528

529

530

531 **Acknowledgements-**

532 We wish to thank the Captain and crew of the Coriolis II for their help during a trying research
533 cruise. We also wish to acknowledge the help of Gilles Desmeules and Sylvain Blondeau for their
534 dedicated electronic and field sampling support as well as Dr. Michel Starr, Qiang Chen, Liliane
535 St-Amand, Sonia Michaud, Hourssem Gaalloul, Jory Cabrol, Robin Bénard, Honghai Zhang for
536 their help in field data acquisition. Most of the plots in this study were created with the ODV
537 Software [Schlitzer, 2009]. This research was funded by a Team grant from the Fonds Québécois
538 de recherche nature et technologies (FQRNT-Équipe-165335) and a Ship-Time Allocation grant
539 from the Natural Sciences and Engineering Research Council of Canada (NSERC-STAC-436804-
540 2013). Finally, we would like to thank the journal reviewers for their constructive comments.

541 **References**

- 542 Andersen, S., Grefsrud, E.S. and Harboe, T. 2013. Effect of increased $p\text{CO}_2$ levels on early shell
543 development in great scallop (*Pecten maximus* Lamarck) larvae. *Biogeosci.* 10: 6161-6184.
544
- 545 Archambault, P., and Goudreau, P. 2006. Effect of the commercial fishery on the Ile Rouge Iceland
546 scallop (*Chlamys islandica*) bed in the St. Lawrence estuary: assessment of the impacts on scallops
547 and the benthic community. DFO Can. Sci. Advis. Sec. Res. Doc. 2006/079.
548
- 549 Barth, J.A.C., and Veizer, J. 1999. Carbon cycle in St Lawrence aquatic ecosystems at Cornwall
550 (Ontario), Canada: seasonal and spatial variations. *Chem. Geol.* **159**: 107–128.
551
- 552 Barwell-Clarke, J., and Whitney, F. 1996. Institute of Ocean Sciences Nutrient Methods and
553 Analysis. Can. Tech. Rep. Hydrogr. Ocean Sci. 182: vi + 43 p.
554
- 555 Bauer, J.E., Cai, W.-J., Raymond, P.A., Bianchi, T.S., Hopkinson, C.S., and Regnier, P.A. 2013.
556 The changing carbon cycle of the coastal ocean, *Nature* **504**: 61–70.
- 557 Bélanger, C. 2003. Observation and Modelling of a Renewal Event in the Saguenay Fjord. Ph.D.
558 thesis, Institut des Sciences de la Mer de Rimouski, Université du Québec à Rimouski, Rimouski,
559 QC, 235 pp.
- 560 Bellis, A. 2002. Spectrophotometric determination of pH in estuarine waters using Phenol Red.
561 B.Sc. Thesis, Department of Earth and Planetary Sciences, McGill University, 53pp.
- 562 Belzile, M., Galbraith, P.S., and Bourgault, D. 2015. Water renewals in the Saguenay Fjord. *J.*
563 *Geophys. Res. Oceans* **120**: 1-20 doi:10.1002/2015JC011085
- 564 Broecker, W.M., and Peng, T-H. 1982. *Tracers in the Sea*, Eldigio Press, Palisades, NY, 690 pp.
565 Bugden, G.L. 1991. Changes in the temperature-salinity characteristics of the deeper waters of the
566 Gulf of St. Lawrence over the past several decades. *In* The Gulf of St. Lawrence: Small Ocean or
567 Big Estuary? Edited by J.-C. Therriault, Can. Spec. Publ. Fish. Aquat. Sci. **113**: 139-147.
- 568 Byrne, R.H. 1987. Standardization of standard buffers by visible spectrometry. *Anal. Chem.* **59**:
569 1479-1481.
- 570 Cai, W.-J., and Wang, Y. 1998. The chemistry, fluxes, and sources of carbon dioxide in the
571 estuarine waters of the Satiala and Altamaha Rivers, Georgia. *Limnol. Oceanogr.* **43**: 657-668.
- 572 Cai, W.-J., Hu, X., Huang, W.-J., Murrell, M. C., Lehrter, J. C., Lohrenz, S. E., Chou, W.-C., Zhai,
573 W., Hollibaugh, J. T., Wang, Y. , Zhao, P., Guo, X. , Gundersen, K., Dai, M., and Gong, G.-C.
574 2011. Acidification of subsurface coastal waters enhanced by eutrophication. *Nature Geosci.* **4**,
575 766–770.
576
- 577 Caldeira, K., and Wickett, M.E. 2005. Ocean model predictions of chemistry changes from carbon
578 dioxide emissions to the atmosphere and ocean. *J. Geophys. Res.-Oceans* **110**: C09S04,
579 doi:10.1029/2004JC002671.

- 580 Chen, C.-T. A., and Borges, A.V. 2009. Reconciling opposing views on carbon cycling in the
581 coastal ocean: Continental shelves as sinks and near-shore ecosystems as sources of atmospheric
582 CO₂. *Deep-Sea Res. II* **56**: 578-590.
- 583 Clayton, T.D., and Byrne, R.H. 1993. Spectrophotometric seawater pH measurements: total
584 hydrogen ion concentration scale calibration of m-cresol purple and at-sea results. *Deep-Sea Res.*
585 **40**: 2115–2129.
- 586
- 587 Clements, J.C., and Hunt, H.L. 2017. Effects of CO₂-driven sediment acidification on infaunal
588 marine bivalves: A synthesis. *Mar. Poll. Bull.* **117**: 6-16.
- 589 Cotovicz Jr., L. C., Knoppers, B. A., Brandini, N., Costa Santos, S. J., and Abril, G. 2015. A strong
590 CO₂ sink enhanced by eutrophication in a tropical coastal embayment (Guanabara Bay, Rio de
591 Janeiro, Brazil), *Biogeosciences* **12**: 6125–6146
- 592 Cyr, F., Bourgault, D., and Galbraith, P.S. 2015. Behavior and mixing of a cold intermediate layer
593 near a sloping boundary. *Ocean Dynamics* **65**: 357-374.
- 594
- 595 Dickie, L., and Trites, R.W. 1983. The Gulf of St. Lawrence. *In Estuaries and Semi-enclosed Seas,*
596 *Edited by L. Dickie and R.W. Trites, Elsevier Scientific Publication, Amsterdam, pp. 403-425.*
- 597 Doney, S.C., Balch, W.M., Fabry, V.J., and Feely, R.A. 2009. Ocean acidification: A critical
598 emerging problem for ocean sciences. *Oceanogr.* **22**: 16-25.
- 599 Dickson, A.G. 1990. Standard potential of the (AgCl + 1/2H₂ = Ag + HCl_(aq)) cell and the
600 dissociation constant of bisulfate ion in synthetic sea water from 273.15 to 318.15 K. *J. Chem.*
601 *Thermodyn.* **22**: 113-127.
- 602 Dinauer, A., and Mucci, A., 2017. Spatial variability of surface-water pCO₂ and gas exchange in
603 the world's largest semi-enclosed estuarine system: St. Lawrence Estuary (Canada).
604 *Biogeosciences* (in press).
- 605 Dupont, S., Dorey, N., Stumpp, M., Melzner, F., and Thorndyke, M. 2013. Long-term and trans-
606 life-cycle effects of exposure to ocean acidification in the green sea urchin *Strongylocentrotus*
607 *droebachiensis*. *Mar. Biol.* **160**: 1835-1843.
- 608 El-Sahb, M.I., and Silverberg, N. 1990. The St. Lawrence Estuary: introduction. *In Oceanography*
609 *of a Large-scale Estuarine System. Edited by M.I. El-Sahb and N. Silverberg, Springer-Verlag,*
610 *New York, pp. 1-9.*
- 611 Fabry, V.J., Seibel, B.A., Feely, R.A., and Orr, J.C. 2008. Impacts of ocean acidification on marine
612 fauna and ecosystem processes. *ICES journal of Mar. Sci.* **65**: 414-432.
- 613 Feely, R. A., Alin, S.R., Newton, J., Sabine, C.L., Warner, M., Devol, A., Krembs, C., and Maloy,
614 C. 2010. The combined effects of ocean acidification, mixing, and respiration on pH and carbonate
615 saturation in an urbanized estuary. *Estuar. Coast. Shelf Sci.* **88**: 442–449.
- 616

- 617 Fortin, G.R., and Pelletier, M. 1995. Synthèse des connaissances sur les aspects physiques et
618 chimiques de l'eau et des sédiments du Saguenay. Environnement Canada Technical Report.,
619 Conservation de l'environnement, Centre Saint-Laurent, Montreal, QC
- 620 Frankignoulle, M., Bourge, I., and Wollast, R. 1996. Atmospheric CO₂ fluxes in a highly polluted
621 estuary (The Scheldt). *Limnol. Oceanogr.* **41**: 365–369.
622
- 623 Frankignoulle, M., Abril, G., Borges, A., Bourge, I., Canon, C., Delille, B., Libert, E., and Théate,
624 J.M. 1998. Carbon dioxide emission from European estuaries. *Science* **282**: 434–436.
625
- 626 Galbraith, P.S. 2006. Winter water masses in the Gulf of St. Lawrence. *J. Geophys. Res. Oceans*
627 **111**: C06022. doi: 10.1029/2005JC003159 Gazeau, F., Gattuso, J.-P., Dawber, C., Pronker, A. E.,
628 Peene, F., Peene, J., Heip, C. H. R., and Middelburg, J. J. 2010. Effect of ocean acidification on
629 the early life stages of the blue mussel *Mytilus edulis*, *Biogeosciences*, **7**: 2051–2060.
630
- 631 Gazeau, F., Parker, L.M., Comeau, S., Gattuso, J.-P., O'Connor, W.A., Martin, S., Pörtner, H.-
632 O., and Ross, P.M., 2013. Impacts of ocean acidification on marine shelled molluscs. *Mar. Biol.*
633 **160**:2207–2245.
634
- 635 Gilbert, D. 2004. Propagation of temperature signals along the northwest Atlantic continental shelf
636 edge and into the Laurentian Channel. *Abstract, ICES CIEM Annual Science Conference*
637 September 22–25, Vigo, Spain.
- 638 Gilbert, D., and Pettigrew, B. 1997. Interannual variability (1948-1994) of the CIL core
639 temperature in the Gulf of St. Lawrence. *Can. J. Fish. Aquat. Sci.* **54**: 57-67.
- 640 Gilbert, D., Gobeil, C., Sundby, B., Mucci, A., and Tremblay, G. 2005. A seventy-two year record
641 of diminishing deep-water oxygen levels in the St. Lawrence estuary: the northwest Atlantic
642 connection. *Limnol. Oceanogr.* **50**: 1654-1666.
- 643 Grasshoff, K., Kremling, K., and Ehrhardt, M. 1999. *Methods of seawater analysis* (3rd ed.).
644 Wiley-VCH, Weinheim, Germany.
645
- 646 Gratton, Y., Mertz, G., and Gagné, J.A. 1988. Satellite observations of tidal upwelling and mixing
647 in the St. Lawrence Estuary. *J. Geophys. Res.* **93**: 6947-6954.
648
- 649 Gratton, Y., Lefavre D., and Couture, M. 1994. Océanographie physique du fjord du Saguenay.
650 *In Le fjord du Saguenay: Un Milieu Exceptionnel de Recherche. Edited by J.-M. Sévigny and C.*
651 *M. Couillard, Ministère des Pêches et des Océans, Institut Maurice-Lamontagne, 8–16.*
- 652 Hansen, H.P., and F. Koroleff F. 2007. Determination of nutrients. *Methods of Seawater Analysis.*
653 Wiley-VCH Verlag GmbH. p. 159-228.
- 654 Holmes, R.M., A. Aminot, R. Kéroue, B.A. Hooker, and B.J. Peterson. 1999. A simple and precise
655 method for measuring ammonium in marine and freshwater ecosystems. *Canadian Journal of*
656 *Fisheries and Aquatic Sciences* **56(10)**:1801-1808.

- 657 Hutin E., Y. Simard, and P. Archambault. 2005. Acoustic detection of a scallop bed from a single-
658 beam echosounder in the St. Lawrence. *ICES J. Mar. Sci.* **62**: 966-983.
- 659 Intergovernmental Panel on Climate Change. 2007. Summary for Policymakers. *In* Climate
660 Change 2007: The Physical Sciences Basis. Working Group I Contribution to the Fourth
661 Assessment Report of the IPCC, *Edited by* S. Solomon, S. et al., Cambridge Univ. Press,
662 Cambridge.
- 663 Karsteen, J. and M. Tomczak, 1999. OMP Analysis Package for Matlab, Version 2.0, Available
664 from <http://omp.geomar.de/>.
665
- 666 Koné, Y. J. M., Abril, G., Kouadio, K. N., Delille, B., and Borges, A. V. 2009. Seasonal variability
667 of carbon dioxide in the rivers and lagoons of Ivory Coast (West Africa), *Estuaries and Coasts*, **32**:
668 246–260.
- 669
- 670 Kroeker, K.J., Kordas, R.L., Crim, R., Hendriks, E., Ramajo, L., Singh, G.D., Duarte, C.M., and
671 Gattuso, J.-P. 2013. Impacts of ocean acidification on marine organisms: quantifying sensitivities
672 and interaction with warming. *Global Change Biol.* 19: 1888-1896.
673
- 674 Kurihara, H. 2008. Effects of CO₂-driven ocean acidification on the early developmental stages
675 of invertebrates, *Mar. Ecol.-Prog. Ser.*, **373**: 275–284.
676
- 677 Lansard, B., Mucci, A., Miller, L.A., Macdonald, R.W., and Gratton, Y. 2012. Seasonal variability
678 of water mass distribution in the southeastern Beaufort Sea determined by total alkalinity and $\delta^{18}\text{O}$.
679 *J. Geophys. Res.-Oceans* **117**: C03003, 19 pp.
680
- 681 Levasseur, M., and Therriault, J.-C. 1987. Phytoplankton biomass and nutrient dynamics in a
682 tidally induced upwelling: the role of the NO₃:SiO₄ ratio. *Mar. Ecol. Prog. Ser.* **39**: 87-97
- 683
- 684 Lewis, E., and Wallace, D.W.R. 1998. Program Developed for CO₂ System Calculations.
685 ORNL/CDIAC-105. Carbon dioxide Information Analysis center, Oak Ridge National Laboratory,
686 US Department of Energy, Oak Ridge, TN. Available from
<http://cdiac.esd.ornl.gov/oceans/co2rprt.html>.
- 687 Locat, J., and Levesque, C. 2009. Le Fjord du Saguenay: Une physiographie et un registre
688 exceptionnels. *Revue des Sciences de l'Eau* **22**: 135-157.
- 689
- 689 Maher, D. T., and Eyre, B. D. 2012. Carbon budgets for three autotrophic Australian estuaries:
690 Implications for global estimates of the coastal air-water CO₂ flux, *Global Biogeochem. Cycles*
691 **26**: GB1032, doi:10.1029/2011GB004075.
- 692
- 692 Macdonald, R.W., Carmack, E. C., McLaughlin, F., Iseki, A.K., Macdonald, D. M., and O'Brien,
693 M.C. 1989. Composition and modification of water masses in the Mackenzie shelf estuary. *J.*
694 *Geophys. Res.* **94**: 18057-18070
- 695
- 695 Mackas, D.L., Denman, K. L., and Bennett, A.F. 1987. Least squares multiple tracer analysis of
696 water mass composition. *J. Geophys. Res.* **92**: 2907-2918.

- 697 Melzner, F., Thomsen, J., Koeve, W., Oschlies, A., Gutowska, M.A., Bange, H.W., Hansen, H.P.,
698 and Körtzinger, A. 2013. Future ocean acidification will be amplified by hypoxia in coastal
699 habitats. *Mar. Biol.* **160**: 1875–1888.
700
- 701 Mertz, G., and Gratton, Y. 1990. Topographic waves and topographically induced motion in the
702 St. Lawrence Estuary, *In Oceanography of a Large-Scale Estuarine System: The St. Lawrence.*
703 M.I El-Sabh and N. Silverberg. vol. 39. New York, Springer-Verlag, pp. 94-108.
- 704 Meybeck, M. 1993. Riverine transport of atmospheric carbon: sources, global typology and
705 budget, *Water Air Soil Poll.* **70**: 443–463.
706
- 707 Miller A. W., Reynolds, A.C., Sobrina, C., and Riedel, G.F. 2009. Shellfish face uncertain future
708 in high CO₂ world: influence of acidification on oyster larvae calcification and growth in estuaries.
709 *PLoS ONE* **4(5)**: e5661, doi:10.1371/journal.pone.0005661.
- 710 Millero, F. J. 1986. The pH of estuarine waters. *Limnol. Oceanogr.* **34**: 839-847.
- 711 Millero, F.J. 2013. *Chemical Oceanography*, 4th Edition, CRC Press, Boca Raton, 469 pp.
- 712 Mucci, A. 1983. The solubility of calcite and aragonite in seawater at various salinities,
713 temperatures and one atmosphere total pressure. *Amer. Jour. Sci.* **283**: 780-799.
- 714 Mucci, A., Richard, L.-F., Lucotte, M., and Guignard, C. 2000. The differential geochemical
715 behavior of arsenic and phosphorus in the water column and sediments of the Saguenay Fjord
716 Estuary, Canada. *Aquat. Geochem.* **6**: 293-324.
- 717 Mucci, A., Starr, M., Gilbert, D., and Sundby B. 2011. Acidification of Lower St. Lawrence
718 Estuary bottom waters. *Atmosphere-Ocean* **49**: 206-213.
719
- 720 Observatoire Global du Saint-Laurent-OGSL, Available from <http://ogsl.ca>, (data downloaded on
721 October 16, 2014).
722
- 723 Osafune, S., and Yasuda, I. 2006. Bidecadal variability in the intermediate waters of the
724 northwestern subarctic Pacific and the Okhotsk Sea in relation to 18.6-year period nodal tidal
725 cycle. *J. Geophys. Res.* **111**: C05007, 14 pp.
726
- 727 Parker, L. M., Ross, P. M., O'Connor, W. A., Borysko, L., Raftos, D. A., and Pörtner, H.-O.
728 2012. Adult exposure influences offspring response to ocean acidification in oysters, *Glob.*
729 *Change Biol.*, **18**: 82–92
730
- 731
- 732 Pierrot, D., E. Lewis, E., and D. Wallace, 2006. MS Excel Program Developed for CO₂ System
733 Calculations. ORNL/CDIAC-105a, Carbon Dioxide Information Analysis Center, Oak Ridge
734 National Laboratory, U.S. Department of Energy, Oak Ridge, Tennessee.
735
- 736 Raymond, P. A., and Cole, J. J. 2001. Gas exchange in rivers and estuaries: Choosing a gas transfer
737 velocity. *Estuaries and Coasts* **24(2)**: 312–317.

- 738 Raymond P.A., Caraco, N.F., and Cole, J.J. 1997. Carbon dioxide concentration and atmospheric
739 flux in the Hudson River. *Estuaries* **20**: 381–390.
740
- 741 Redfield A.C., Ketchum, B.H., and Richards, F. A. 1963. The influence of organisms on the
742 composition of sea water, *In The sea*, Vol. 2, Edited by M. N. Hill, pp. 26–77. Wiley.
- 743 Regnier, P., Friedlingstein, P., Ciais, P., Mackenzie, F.T., Gruber, N., Janssens, I.A., Laruelle,
744 G.G., Lauerwald, R., Luyssaert, S., Andersson, A.J., Arndt, S., Arnosti, C., Borges, A.V., Dale,
745 A.W., Gallego-Sala, A., Godd ris, Y., Goossens, N., Hartmann, J., Heinze, C., Ilyina, T., Joss, F.,
746 LeRowe, D.E., Liefeld, J., Meysman, F.J.R., Munhoven, G., Raymond, P.A., Spahni, R.,
747 Suntharalingam, P., and Thullner, M. 2013. Anthropogenic perturbation of the carbon fluxes from
748 land to ocean, *Nat. Geosci.*, 6: 597–607
- 749 Ries, J. B., Cohen, A.L. and McCorkle, D.C. 2009. Marine calcifiers exhibit mixed responses to
750 CO₂-induced ocean acidification. *Geology* **37**: 1131-1134.
- 751 Robert-Baldo, G., Morris, M.J., and Byrne, R.H. 1985. Spectrophotometric determination of
752 seawater pH using phenol red. *Anal. Chem.* **57**: 2564-2567.
- 753 Sabine, C.L., Feely, R.A., Gruber, N., Key, R.M., Lee, K., Bullister, J.L., Wanninkof, R., Wong,
754 C.S., Wallace, D.W.R., Tilbrook, B., Millero, F.J., Peng, T.-H., Kozyr, A., Ono, T., and Rios, A.
755 2004. The oceanic sink for anthropogenic CO₂. *Science* **305**: 367-371.
- 756 Saucier, F.J., and Chass , J. 2000. Tidal circulation and buoyancy effects in the St. Lawrence
757 Estuary. *Atmosphere-Ocean* **38**: 505-556.
758
- 759 Schafer, C.T., Smith, J.N., and C t , R. 1990. The Saguenay Fjord: A major tributary to the St.
760 Lawrence Estuary. *In Oceanography of a Large-Scale Estuarine System: The St. Lawrence*. M.I
761 El-Sabh and N. Silverberg. vol. 39. New York, Springer-Verlag, pp. 378-420.
- 762 Schlitzer, R. 2009. Ocean Data View, <http://odv.awi.de/>, Alfred Wegener Inst. for Polar Mar. Res.,
763 Bremerhaven, Germany.
764
- 765 Siebert, G.H., Trites, R.W., and Reid, S.J. 1979. Deepwater exchange processes in the Saguenay
766 Fjord. *J. Fish. Res. Board Can.* **36**: 42-53.
- 767 Stacey, M.W., and Gratton, Y. 2001. The energetics and tidally induced reverse renewal in a two-
768 silled fjord. *J. Phys. Oceanogr.* **31**: 1599-1615.
- 769 Sunda W. G., and Cai, W.-J. 2012. Eutrophication induced CO₂-acidification of subsurface coastal
770 waters: interactive effects of temperature, salinity, and atmospheric pCO₂. *Environ. Sci. Technol.*
771 **46**: 10651–10659.
772
- 773 Stumm W., and Morgan J. J. 1996. *Aquatic Chemistry: Chemical Equilibria and Rates in Natural*
774 *Waters*. 3rd ed., John Wiley & Sons, Inc., New York, NY, 780 pp.
775

- 776 Taguchi, F., and Fujiwara, T. 2010. Carbon dioxide stored and acidified low oxygen bottom waters
777 in coastal seas, Japan. *Estuar. Coast. Shelf Sci.* **86**: 429–433.
778
- 779 Talmage, S. C. and Gobler, C. J.: Effects of past, present, and future ocean carbon dioxide
780 concentrations on the growth and survival of larval shellfish, *Proc. Natl. Acad. Sci.* **107**: 17246–
781 17251.
782
- 783 Tate, R.D., Benkendorff, K., Lah R.A., and Kelaher, B.P. 2017. Ocean acidification and
784 warming impacts the nutritional properties of the predatory whelk, *Dicathais orbita*. *J. Exp. Mar.*
785 *Biol. Ecol.* **493**: 7-13.
786
- 787 Therriault J.-C., and Lacroix, G. 1977. Penetration of the deep layer of the Saguenay Fjord by
788 surface waters of the St-Lawrence Estuary. *J. Fish. Res. Board Can.* **112**: 77-96.
- 789 Therriault J.-C., and Levasseur, M. 1985. Control of phytoplankton production in the lower St.
790 Lawrence estuary: Light and freshwater runoff. *Nat. Can.* **112**: 77-96.
- 791 Tomczak, M., 1981. A multiparameter extension of temperature/salinity diagram techniques for
792 the analysis of non-isopycnal mixing. *Prog. in Oceanogr.* **10**:147-171.
- 793 Uppström, L.R. 1974. The boron/chlorinity ratio of deep-sea water from the Pacific Ocean. *Deep*
794 *Sea Research and Oceanographic Abstracts* 21, 161-162.
795
- 796 Uthicke, S., Ebert, T., Liddy, M., Johansson, C., Fabricius, K.E., and Lamare, M. 2016.
797 *Echinometra* sea urchins acclimatized to elevated $p\text{CO}_2$ at volcanic vents outperform those under
798 present-day $p\text{CO}_2$ conditions. *Global Change Biol.* **22**: 2451-2461.
799
- 800 Wallace R.B., Baumann, H., Grear, J.S., Aller, R.C., and Gobler, C.J. 2014. Coastal ocean
801 acidification: the other eutrophication problem. *Estuar. Coast. Shelf Sci.* **148**, 1–13.
802
- 803 Wang X., and Veiser, J. 2000 Respiration-photosynthesis balance of terrestrial aquatic
804 ecosystems, Ottawa area, Canada. *Geochim. Cosmochim. Acta* 64: 3775-3786.
805
- 806 Wanninkhof, R. 2014. Relationship between wind speed and gas exchange over the ocean
807 revisited. *Limnol. Oceanogr. Methods*, 12(6): 351–362.
- 808
- 809 Yang C., Telmer, K., and Veiser, J. 1996. Chemical dynamics of the “St. Lawrence” riverine
810 system: $\delta\text{D}_{\text{H}_2\text{O}}$, $\delta^{18}\text{O}_{\text{H}_2\text{O}}$, $\delta^{13}\text{C}_{\text{DIC}}$, $\delta^{34}\text{S}_{\text{sulfate}}$, and dissolved $^{87}\text{Sr}/^{86}\text{Sr}$. *Geochim. Cosmochim. Acta*
811 **60**: 851-866.
812
- 813 Zakardjian B.A., Gratton Y. and Vézina A.F. 2000. Late spring phytoplankton bloom in the Lower
814 St. Lawrence Estuary: the flushing hypothesis revisited. *Mar. Ecol. Prog. Ser.* **192**: 31-48.
- 815

816 Zeebe, R.E., and Wolf-Gladrow, D. 2001. CO₂ in Seawater: Equilibrium, Kinetics, Isotopes,
817 Amsterdam, Elsevier Science, Elsevier Oceanography Series, 346 pp.

818

819

820

821

Draft

822 **Figure 1- a)**

823

824

825

826

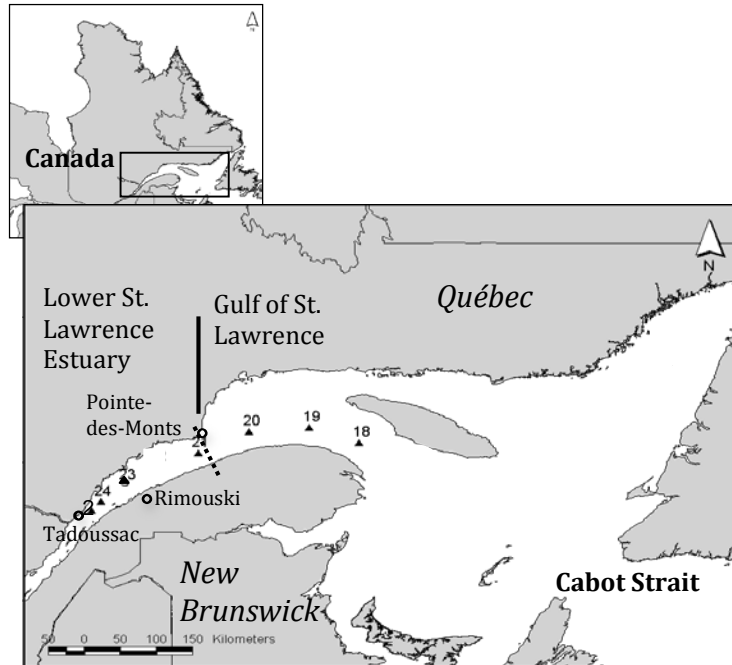
827

828

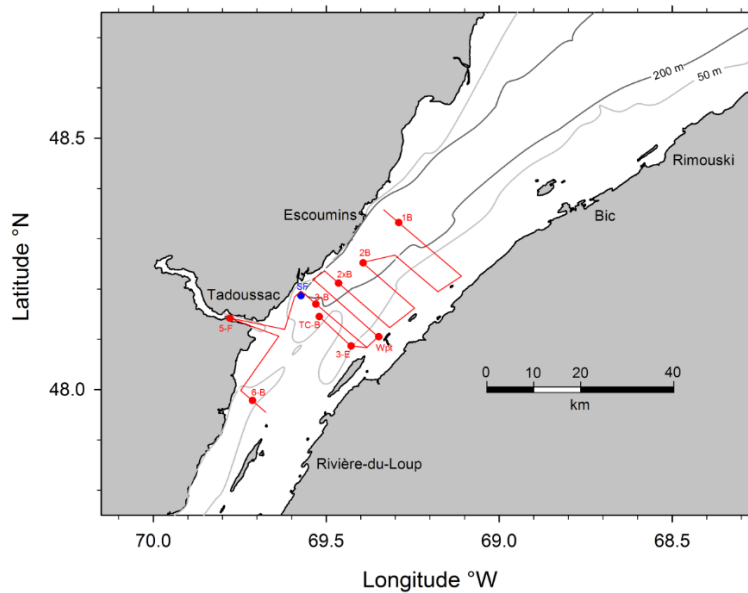
829

830

831

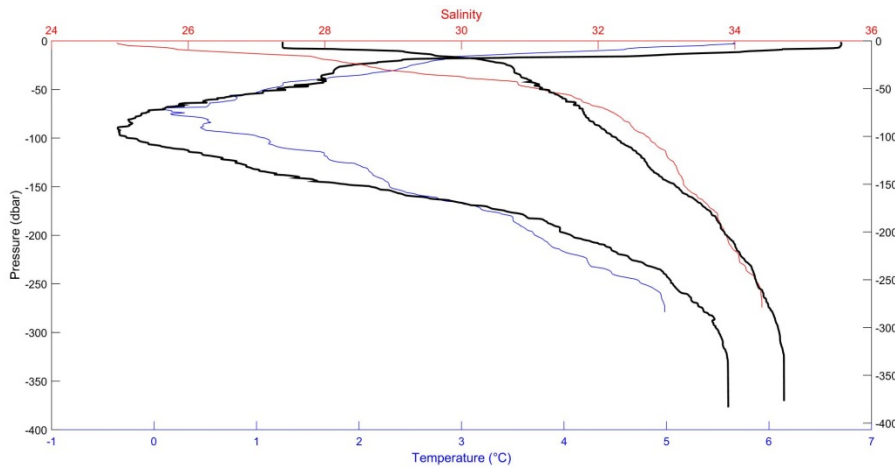


832

833 **Figure 1- b)**

834

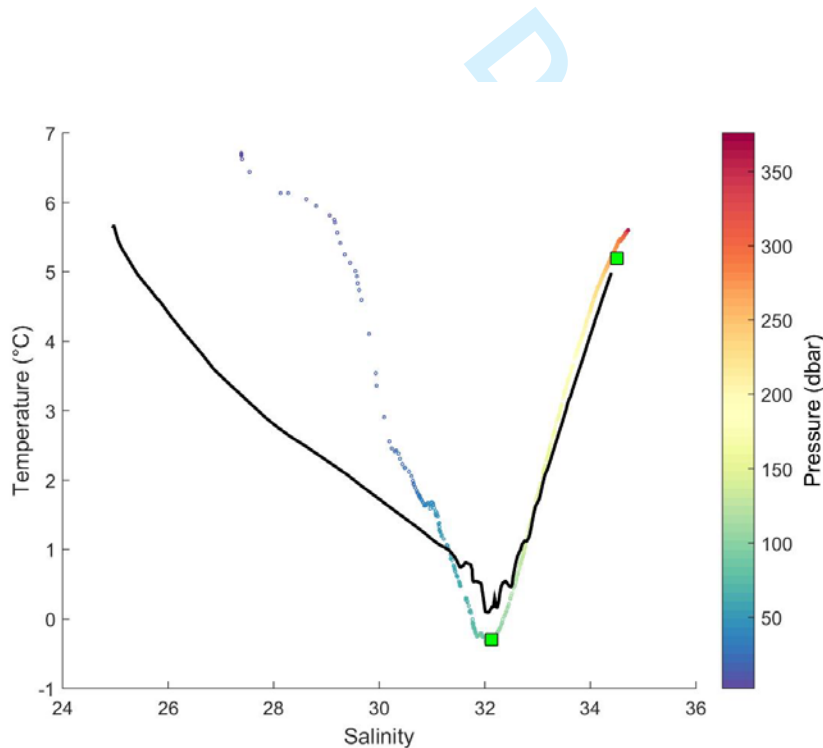
835 **Figure 1.** a) Map of the St. Lawrence Estuary and location of stations visited on a cruise
 836 immediately prior to this study (June 3-8, 2013) as well as b) the transect track and position of
 837 the fixed sampling station visited during this study (June 10-15, 2013). Water properties
 838 measured on the previous cruise and along the transect were used to define the water-type
 839 properties and served for the water mass analysis in OMP

840 **Figure 2 –**841 **a)**

842

843 **b)**

844

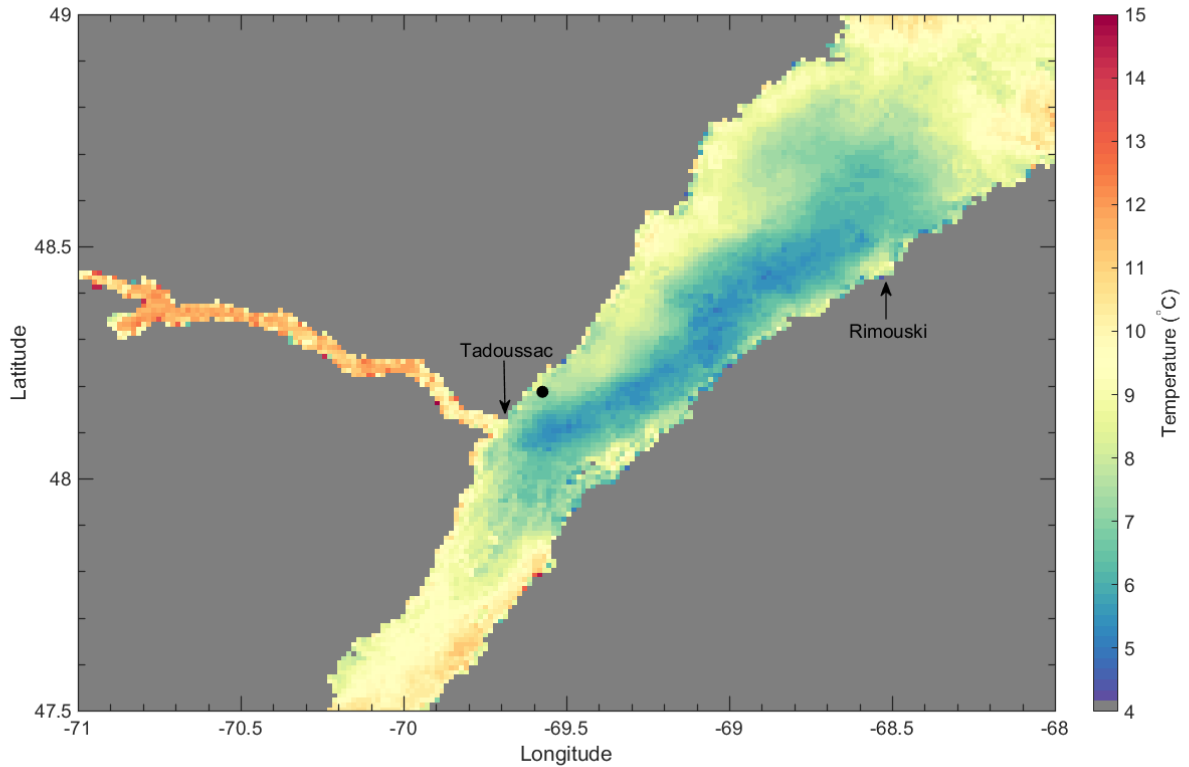


845 **Figure 2.** a) Vertical profiles of the salinity (red line) and temperature (blue line) throughout the
 846 water column as recorded at the fixed station on June 11, 2013 at 16:48 GMT. We also show the
 847 profiles (thick black lines) from station 18. The data are reproduced in a T-S diagram (b) that
 848 reflects the three-layer estuarine circulation in the Lower St. Lawrence Estuary. The green
 849 squares indicate the CIL and LSLE bottom-water endmembers.

850

851 **Figure 3 -**

852



853

854 **Figure 3.** Three-day (June 13-15, 2013) average sea surface temperature during the fixed station
855 (black dot) measurements (OGSL 2014).

856

857

858

Figure 4 -

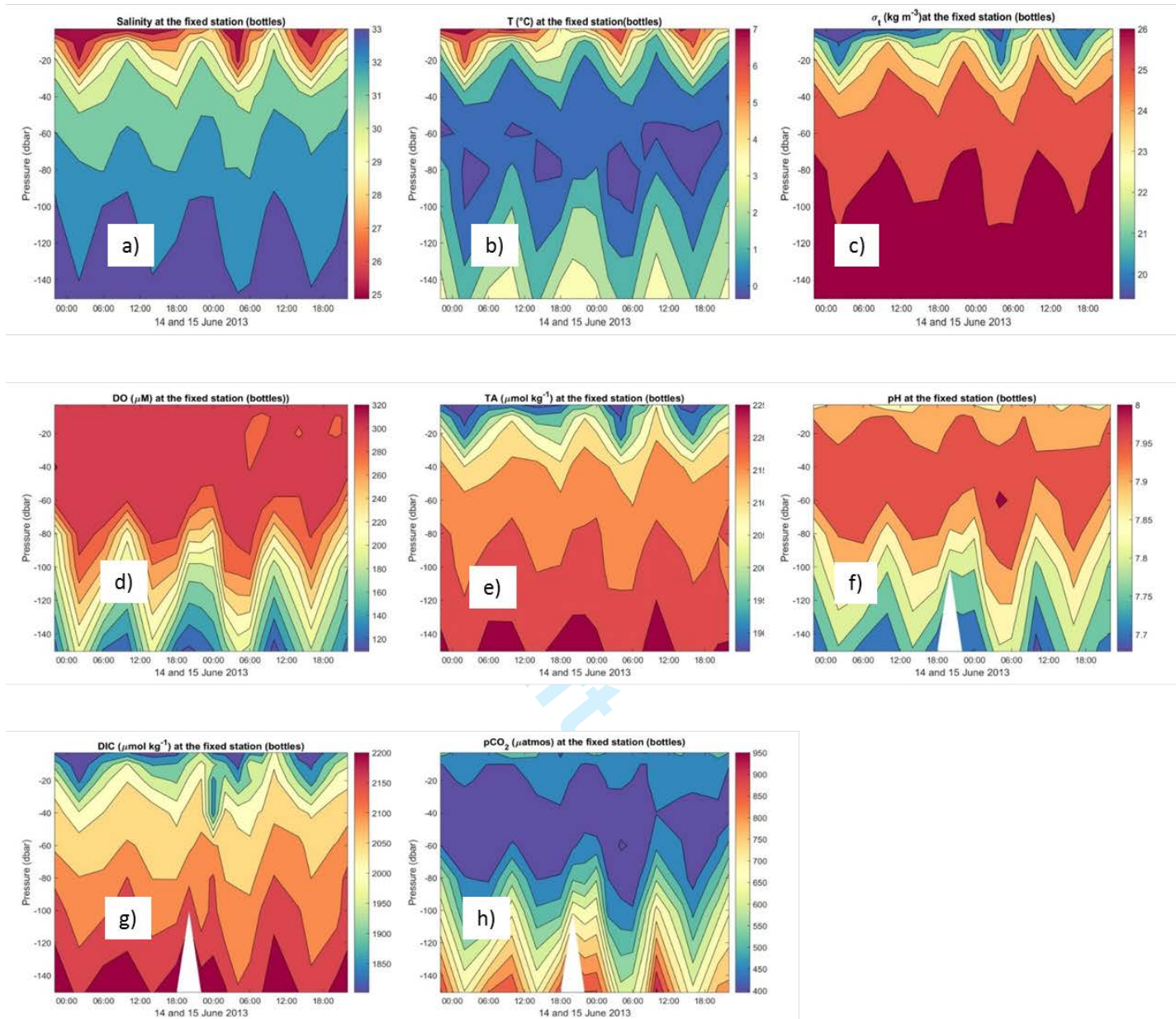


Figure 4. Water properties measured at the fixed station (48°11.2'N, 69°34.4'W) over two tidal cycles, June 14-15, 2013: a) Practical Salinity, b) Temperature, c) Sigma-t, d) Dissolved Oxygen, e) Titration alkalinity (TA), f) pH_T, g) Dissolved inorganic carbon (DIC, calculated from TA and pH_T), h) pCO₂ (calculated from TA and pH_T). All panels were plotted from discrete samples (~ 3, 10, 20, 40, 60, 80, 100 and 150 m) taken from the Niskin bottles. Dissolved nitrate, nitrite, silicate, and soluble reactive phosphate (SRP) data can be found in the electronic attachment.

Figure 5 –

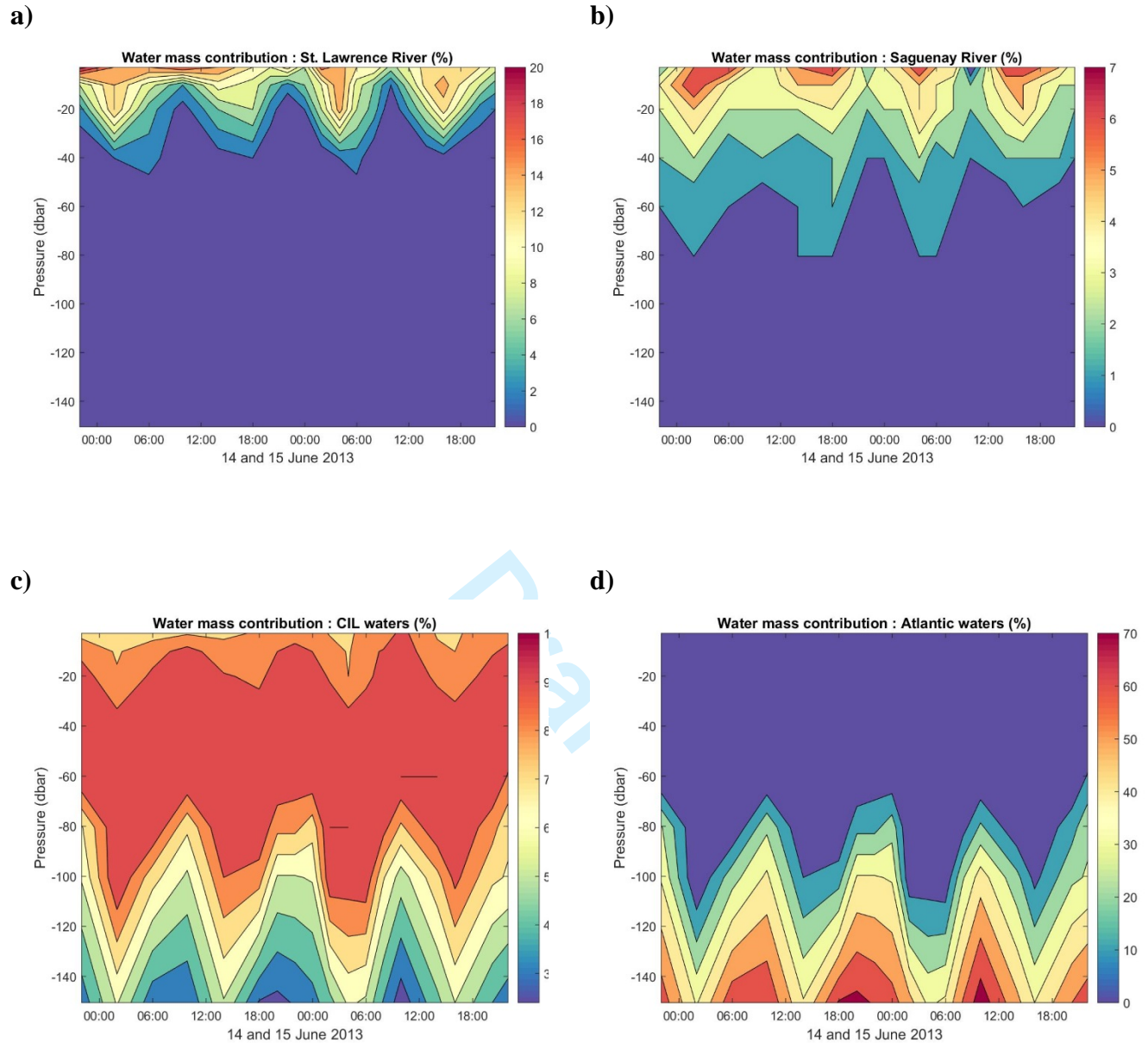
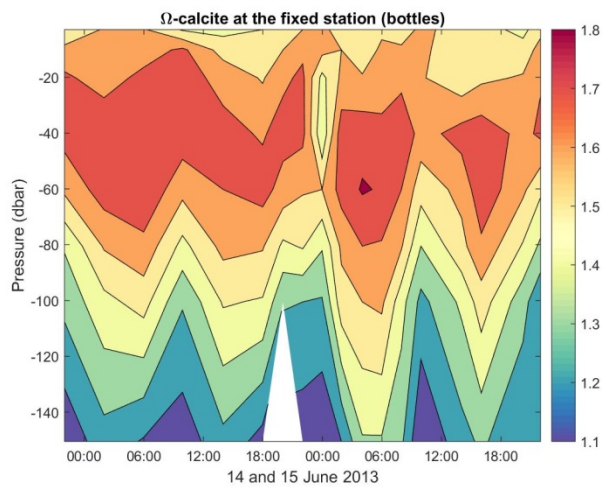


Figure 5. Distribution (%) of water-source types at the fixed station ($48^{\circ}11.2'N$, $69^{\circ}34.4'W$) over two tidal cycles, June 13-15, 2013: a) St. Lawrence River water, b) Saguenay River water, c) cold intermediate layer (CIL) water, d) Lower St. Lawrence Estuary (LSLE) bottom water or Atlantic water.

Figure 6-

a)



b)

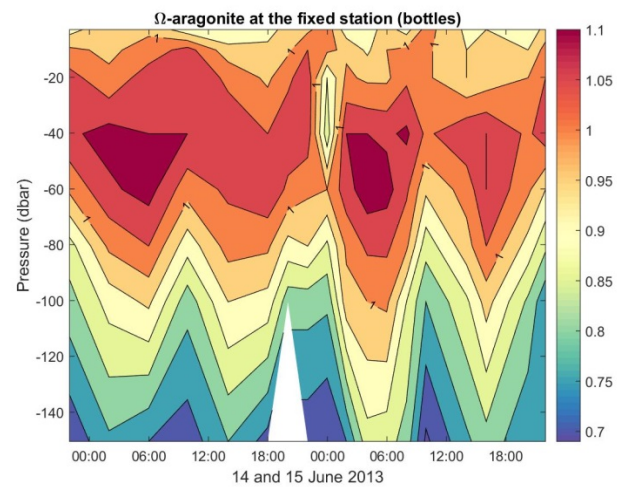


Figure 6. Saturation state of the water column with respect to a) calcite and b) aragonite at the fixed station (48°11.2'N, 69°34.4'W) over two tidal cycles, June 14-15, 2013.

Figure 7-

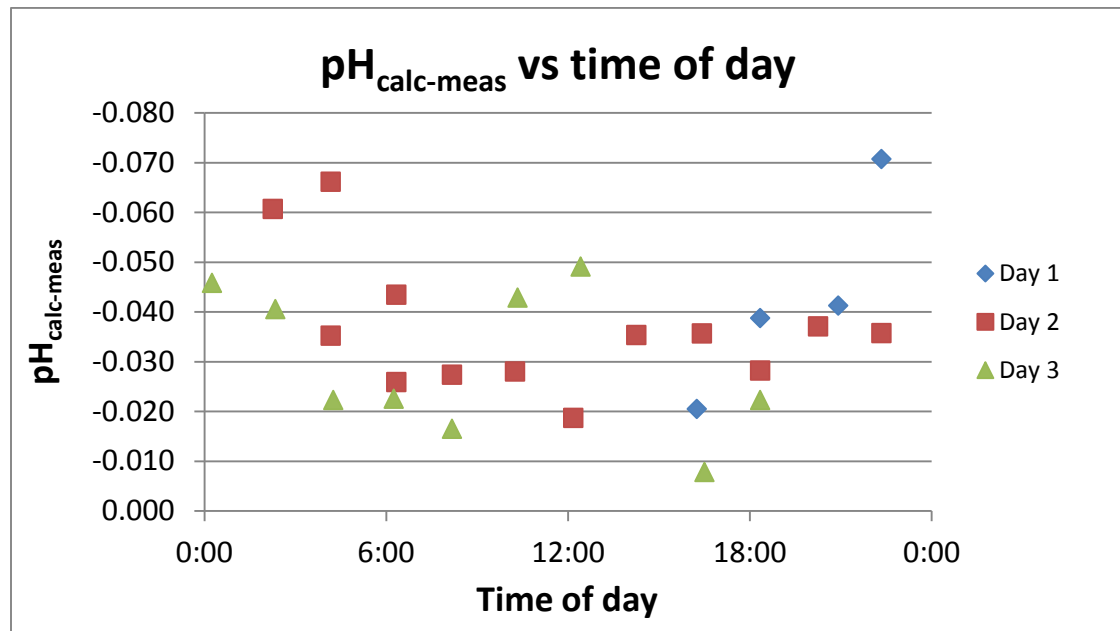


Figure 7 – Difference between calculated (based on conservative mixing of the four source water types) and measured pH_T values in the surface waters at the fixed station as a function of the time of day over two full tidal cycles over three consecutive days (see Table 2 for details). Errors originate mostly from the variance on the fractional contributions obtained from the OMP analysis and, in this specific situation on the fractional contribution of the Saguenay River water (most divergent TA and pH). Although typically on the order of 10% (Lansard et al. 2012), we applied a +50% error to this value and the difference in computed pH_T was less than 0.003 unit, below the uncertainty of our field measurements and smaller than the size of the symbols.

Table 1. Source water types and their characteristic properties used in the OMP analysis

Water types	T (°C)	S _P	δ ¹⁸ O (‰)	TA ---(μmol kg ⁻¹)--	DIC ¹	DO	ΣSi ----- (μmol L ⁻¹) -----	SRP ----- (μmol L ⁻¹) -----	DIN	pCO ₂ (μatm)	pH _t
St. Lawrence River	15	0	-9.61	1000	1022	300	45 ²	0.7 ²		575	8.11 ³
Saguenay River	12	0	-13.14	80	97	320	78 ²	1.2 ²		340	7.12 ³
CIL	-0.3	32.13	-1.64	2183	2108	295	10.5	1.1	9.8	450	7.97
LSLE Bottom water	5.2	34.51	-0.28	2296	2165	63.5	52.2	2.4	22.8	1400	7.62

TA – titration alkalinity, DIC – dissolved inorganic carbon, DO – dissolved oxygen, ΣSi – dissolved silicate, SRP – soluble reactive phosphate, DIN – dissolved inorganic nitrogen
¹ DIC values were not measured directly, but calculated from pH and TA using the Excel version of CO2SYS (Pierrot et al., 2006) for the marine waters and the web-based version of PHREEQC (www.ndsu.edu/webphreeq/) for the freshwaters.

² Values were not measured at the time of sampling, they are averages of measurements carried out in the previous 5 years at similar times of the year.

³ pH of freshwaters were not measured at the time of sampling, values that appear in the table are averages of measurements carried out in the previous 5 years at similar times of the year on the NBS scale (infinite dilution convention).

Table 2. Weight applied to each parameter used in the OMP analysis

Parameters	Precision	Weights used in OMP analysis	
		Above the CIL	Below the CIL
Temperature (°C)	0.01	1	25
Practical salinity	0.01	25	25
Dissolved O ₂ (μmol L ⁻¹)	2.0	1	5
Total alkalinity (μmol kg ⁻¹)	2.0	25	25
δ ¹⁸ O(H ₂ O) (‰)	0.05	25	25
Mass conservation		25	25

Table 3. Reconstructed surface water properties at the fixed station (SF) (conservative mixing of source-water types according to the OMP results) over two full tidal cycles (June 13-15, 2013) and differences between the calculated and observed values.

Time	Depth (m)	pH _T	DIN ----- μmol/L	SRP ----- μmol/L	ΣSi -----	DO	ΔpH _T	ΔDIN ----- μmol/L	ΔSRP ----- μmol/L	ΔSi -----	ΔDO -----
16:15	3.2	7.833	13.5	1.06	18.5	297	-0.021	-5.1	0.21	-3.9	-10
18:20	3.1	7.840	13.6	1.02	19.0	297	-0.039	1.3	0.26	-2.6	-16
20:55	3.1	7.841	14.2	1.05	20.0	297	-0.041	-9.2	0.29	-1.6	-13
22:20	2.9	7.849	14.3	1.04	20.3	297	-0.071	5.4	0.28	-1.3	-14
1+ 0:10	3.2	7.856	13.9	1.04	19.6	297	-0.047	1.3	0.28	-2.0	-11
1+ 2:15	2.8	7.858	14.6	1.04	21.0	298	-0.061	-1.6	0.43	-0.9	-12
1+ 4:10	1.2	7.861	13.9	1.05	19.5	297	-0.066	8.8	0.44	-1.5	-4
1+ 4:10	3.1	7.889	12.9	1.09	17.1	297	-0.035	-14.8	0.47	-3.9	-9
1+ 6:20	1.3	7.840	14.6	1.04	20.9	297	-0.043	0.8	0.32	-0.7	-5
1+ 6:20	3.2	7.837	13.6	1.03	19.0	297	-0.026	-7.7	0.39	-2.0	-10
1+ 8:10	3.1	7.853	13.9	1.04	19.5	297	-0.027	-8.0	0.40	-1.5	-14
1+ 10:15	3.2	7.861	14.1	1.04	20.0	297	-0.028	-5.5	0.40	-1.3	-13
1+ 12:10	2.7	7.841	14.2	1.04	20.2	297	-0.019	-8.2	0.34	0.2	-14
1+ 14:15	2.8	7.904	13.9	1.06	19.4	297	-0.035	3.8	0.26	0.2	-10
1+ 16:25	3.0	7.886	12.9	1.06	17.1	297	-0.036	0.7	0.09	0.2	-5
1+ 18:20	3.5	7.885	12.4	1.05	16.3	296	-0.028		0.19	-3.3	-8
1+ 20:15	3.1	7.864	12.2	1.07	15.8	296	-0.037		0.14	-2.4	-11
1+ 22:20	3.0	7.861	13.8	1.04	19.3	297	-0.036	2.6	0.29	-3.3	-10
2+ 0:15	2.6	7.852	14.3	1.05	20.3	297	-0.046	-0.3	0.31	0.8	-13
2+ 2:20	2.9	7.880	13.1	1.06	17.7	297	-0.041	1.9	0.33	-3.2	-7
2+ 4:15	3.2	7.874	13.3	1.06	18.2	297	-0.022	-5.0	0.20	-0.3	-10
2+ 6:15	3.1	7.910	10.9	1.07	13.0	296	-0.023	11.3	0.06	-0.9	-5
2+ 8:10	3.3	7.856	12.5	1.06	16.4	296	-0.017	-5.4	0.14	-0.7	-8
2+ 10:20	3.3	7.847	14.2	1.05	20.0	298	-0.043	1.1	0.27	0.1	-9
2+ 12:25	3.2	7.861	14.3	1.05	20.2	298	-0.049	1.9	0.26	-0.1	-8
2+ 16:30	3.2	7.883	13.1	1.06	17.6	297	-0.008	-7.6	0.19	-2.3	-8
2+ 18:20	2.7	7.885	12.3	1.07	16.0	296	-0.022	-0.8	0.28	1.4	-7

Figure captions -

Figure 1. a) Map of the St. Lawrence Estuary and location of stations visited on a cruise immediately prior to this study (June 3-8, 2013) as well as b) the transect track and position of the fixed sampling station visited during this study (June 10-15, 2013). Water properties measured on the previous cruise and along the transect were used to define the water-type properties and served for the water mass analysis in OMP.

Figure 2. a) Vertical profiles of the salinity (red line) and temperature (blue line) throughout the water column as recorded at the fixed station on June 11, 2013 at 16:48 GMT. We also show the profiles (thick black lines) from station 18. The data are reproduced in a T-S diagram (b) that reflects the three-layer estuarine circulation in the Lower St. Lawrence Estuary.

Figure 3. Three-day (June 13-15, 2013) average sea surface temperature during the fixed station (black dot) measurements (OGSL 2014).

Figure 4. Water properties measured at the fixed station ($48^{\circ}11.2'N$, $69^{\circ}34.4'W$) over two tidal cycles, June 14-15, 2013: a) Practical Salinity, b) Temperature, c) Sigma-t, d) Dissolved Oxygen, e) Titration alkalinity (TA), f) pH_T , g) Dissolved inorganic carbon (DIC, calculated from TA and pH_T), h) pCO_2 (calculated from TA and pH_T). All panels were plotted from discrete samples (~ 3, 10, 20, 40, 60, 80, 100 and 150 m) taken from the Niskin bottles.

Figure 5. Distribution (%) of water-source types at the fixed station ($48^{\circ}11.2'N$, $69^{\circ}34.4'W$) over two tidal cycles, June 13-15, 2013: a) St. Lawrence River water, b) Saguenay River water, c) cold intermediate layer (CIL) water, d) Lower St. Lawrence Estuary (LSLE) bottom water or Atlantic water.

Figure 6. Saturation state of the water column with respect to a) calcite and b) aragonite at the fixed station ($48^{\circ}11.2'N$, $69^{\circ}34.4'W$) over two tidal cycles, June 14-15, 2013.

Figure 7 – Difference between calculated (based on conservative mixing of the four source water types) and measured pH_T values in the surface waters at the fixed station as a function of the time of day over two full tidal cycles over three consecutive days (see Table 2 for details). Errors originate mostly from the variance on the fractional contributions obtained from the OMP analysis and, in this specific situation on the fractional contribution of the Saguenay River water (most divergent TA and pH). Although typically on the order of 10% (Lansard et al. 2012), we applied a +50% error to this value and the difference in computed pH_T was less than 0.003 unit, below the uncertainty of our field measurements and smaller than the size of the symbols.

Supplemental material –

Fig S1.

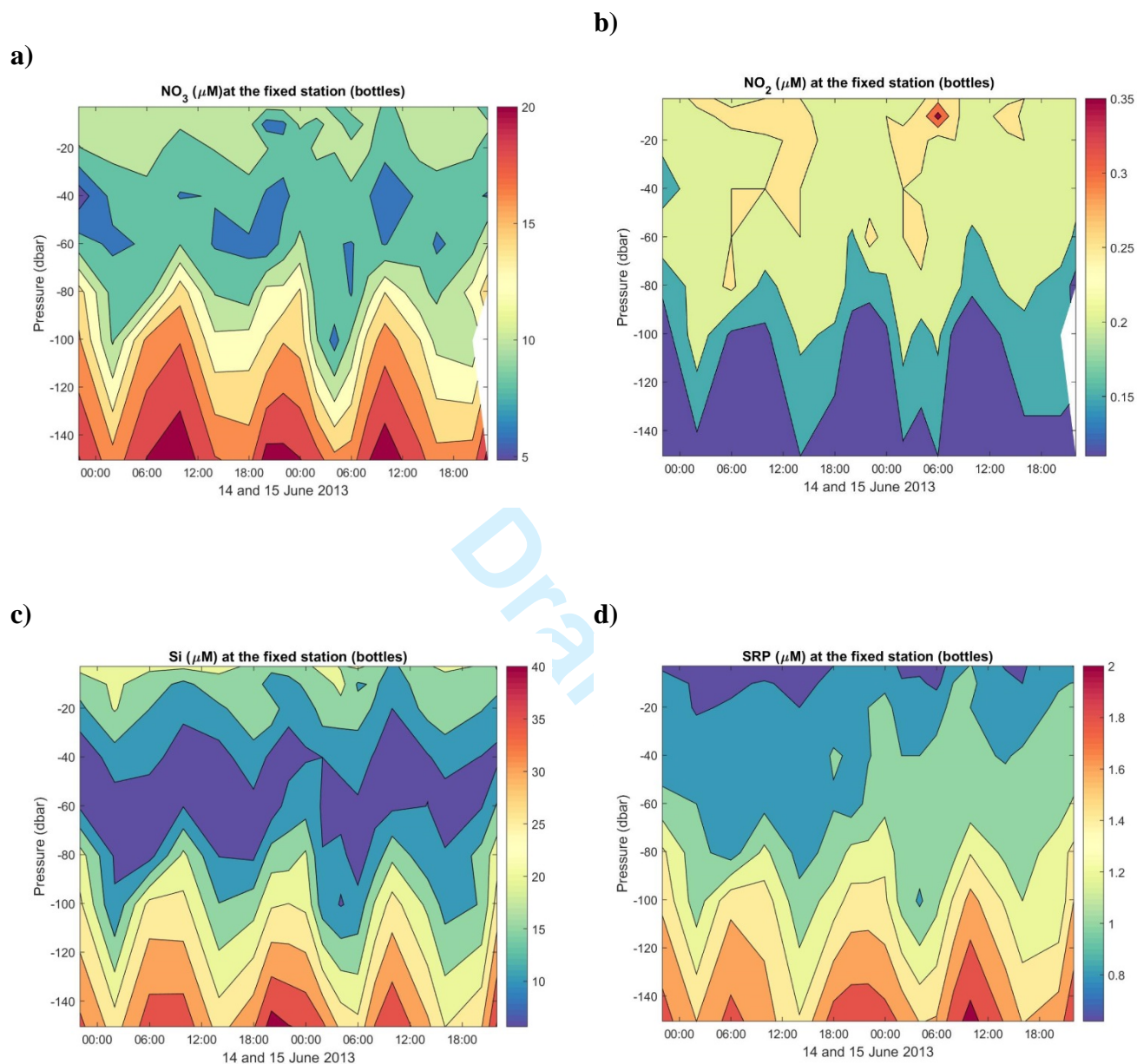


Figure S1. Water properties measured at the fixed station (48°11.2'N, 69°34.4'W) over two tidal cycles, June 14–15, 2013: a) Dissolved nitrate, b) Dissolved nitrite, c) Dissolved silicate, d) Soluble reactive phosphate (SRP). All panels were plotted from discrete samples (~ 3, 10, 20, 40, 60, 80, 100 and 150 m) taken from the Niskin bottles.